Dear Kenny Matsuoka, TC editorial board, and reviewers,

We thank you a lot for your useful comments and suggestions. You can find bellow our modifications to the manuscript following your recommandation (in bold). We hope we answered all your comments, but we would be happy to clarify further the manuscript if needed.

With our best wishes for the upcoming new year,

Cécile Agosta, on behalf of all co-authors

The revised manuscript is associated with 13 supplemental figures and 2 tables. This helps readers to get the comprehensive understanding of this work, but it requires a lot of cross-referring. In some cases, extra few sentences in the main text could help readers understand the contents without cross-referring the supplement. Please review the entire manuscript to see (1) whether arguments in the supplement are cited at the right position (rather than as an addition at the end of the discussion for completeness), and (2) whether the main text summarizes the materials presented in the supplement (if not, add a few sentences to help readers). This is the case for snow drift analysis using surface curvature and wind speed. When I read the manuscript pages 11-12 and see Figures 4, S11 and S12, I was not convinced why these wind threshold values are chosen. Then, at P12 L19, Table S2 is refereed, in which I found more detail analysis for different wind speed thresholds.

We clarified the paragraph about wind thresholds :

"We propose that drifting snow transport fluxes (ds_{tr}) not resolved by MAR can be estimated as a scaling of curvature depending of wind speed: $ds_{tr} = \alpha(ws_{10}) \cdot$ curvature (Figure 4b). The scaling factor $\alpha(ws_{10})$ depends on wind thresholds to simulate the transition between no drifting snow transport for low wind speed ($\alpha = 0$ for $ws_{10} < 5$ m s^{-1}) and drifting snow transport scaled to curvature for high wind speed ($\alpha = 3700\ 10^6$ kg m^{-1} yr^{-1} for $ws_{10} > 9$ m s^{-1}), with a linearly increasing scaling factor between 5 and 9 m s^{-1} for a smooth transition around the 7 m s^{-1} wind threshold defined above. That estimate of drifting snow transport fluxes shows little sensitivity to the choice of the wind thresholds and of the scaling factor (see fluxes summed over the ice sheet for different thresholds and scaling factors in Table S2). The spatial pattern of drifting snow transport we obtain is comparable to the one simulated by RACMO2 (Fig. 4c), except that it gives fluxes more than three times larger than in RACMO2 (see Table S2, and note the different colour map scales between Fig.4b and 4c)."

We better summarized the material presented in Fig. S4 and S5 (ex. Fig. S13), Fig. S9, and Fig. S10:

"Another noticeable result is that MAR forced by ERA-Interim, JRA-55 and MERRA2 give very similar results for the SMB spatial pattern, not only at the observation locations (Fig. 2) but also at the ice sheet scale (comparisons of MAR SMB for different forcing reanalyses are shown in Fig.S4, with colormap scales 10 time smaller than in Fig.S5 where MAR is compared to RACMO2)"

"As a consequence, the surface wind divergence, which drives the snowdrift mass transport, is strongly related to the curvature of the topography, and both have similar spatial patterns (shown in Fig.S9)"

"For three out of the four transects we find only one shift for which the correlation is significant, and for remaining transect (Syowa--Dome F) we find no significant correlation (Fig.S10)."

I found many typos; I actually spent a lot of time to realize some of them can be a typo**.** One reviewer also pointed out that the reference list has typos and should be carefully checked by the authors. Because of the degree of cross-referring in this manuscript, readers can be easily confused with typos.

[We corrected numerous typo in the text thanks to your suggestions bellow, and in the reference list which has been carefully checked]

I request minor revision; it means that the new manuscript will not be sent to the reviewers but assessed by the editor. Please submit marked manuscript to highlight changes made in the next round. Point-to-point responses are necessary if you don't agree the suggestions or if you change the manuscript largely different from the suggestions.

The manuscript improved significantly with helpful reviews. Thus, I'd suggest the authors to acknowledge these reviewers.

[We agree, thank you for your suggestion.]

Thanks for submitting your work to TCD and I look forward seeing the revised manuscript.

Kenny Matsuoka, TC/TCD Editor

Editorial points:

- P4L1: add unit for snow density. **[corrected]**
- P5L15: what does the hyphen between Fig. 1 and 5% mean? Should it be replaced with comma? **[yes, corrected]**
- P6 Table 1 caption and forward: elevation reference is not shown. Is it reference to the sea level? I am asking this question because the elevations are shown very precisely (to 1 m). If it is referenced to the sea level, rewrite "m" to "m a.s.l." This comment is applicable for all of this problem found elsewhere in the manuscript. **[yes, corrected]**
- P7L5: "scales compared to Fig. S9". Is it Fig. S8, not S9? **[corrected, it was S13 … + more detailed explanation]**
- P8 Figure 2 caption 2-3 lines from the bottom: I cannot see markers with white and black faces. **[clarified]**
- P9 Table 2: Please show the boundary of West and East Antarctic Ice Sheets, as well as the southern boundary of Peninsula in one of maps, probably Fig. 2.

Basins are now shown in Fig.2 and the information is added in Table 2 caption and in Fig. 2 caption.

- P10 Fig. 3: "difference in SMB between models and observation" is ambiguous. Please clarify whether it is "(model) – (observation)" or "(observation) – (model)". **[clarified]**
- P10 Fig. 3: Why does MAR SMB is shifted by -30? Does it mean "0" in the figure means "-30"? If this adjustment is made for the presentation purpose, please do not shift the data but change the y axis label. The green and brown masks are used to show positive and negative values. However, because of this shift, the mask may give a wrong impression. My recommendation is to remove this shift, and expand the y axis range to capture the full variations.

We removed the shift.

- P10L2: Add "local" before "fluctuations" at the beginning of the paragraph. **[corrected]**
- P11 Fig 4 caption: Do you mean "back outlines" by saying "black contours"? **[corrected]**
- P11 Fig. 4 caption line 7th from the top: it is said "wind speed greater than 9 m/s". Is this typo, and supposed to be "greater than 7 m/s"? (I actually spent long time to realize that it can be a typo and wondered why you use two different criteria).

There is no typo but we wanted a smooth increase of the alpha coefficient from 0 (wind speed too weak to induce drifting snow) to 3700 (high wind speeds). As we saw that 7 m/s might be a good threshold for wind speed, we computed this smooth increase around 7 m/s. This explains the 5 to 9 wind speed range, and also why we also use the 6-8 wind speed range in Table S2. We added "and α linearly increasing as a function of wind speed in between*, around the 7 m s^{-1} wind speed threshold.*". We also clarified this point in the main text (see bellow).

- P12 L3-4: here it is said that there is no relationship between SMB and curvature if wind speed is lower than 7 m/s. However, in Fig 4 caption, the drift snow is proportional to the wind speed when the wind speed ranges between 5-7 m/s. Please clarify.

It is for the same reason than above, I hope the change clarify this.

- P12 L6: not elevation curvature, but surface curvature. **[corrected]**
- P12 L19-24: unclear. Revise.

We re-wrote the paragraph, we hope it's now clearer:

"Our drifting snow transport estimate gives a good constraint for drifting snow fluxes above 2000 m a.s.l., where low temperatures induce negligible atmospheric sublimation. As drifting snow transport is proportional to the amount of snow in suspension in the atmosphere, quantifying this flux also enables to constrain the amount of snow eroded from the snowpack to the atmosphere, which drives drifting snow sublimation fluxes at lower elevation. This is of importance as drifting snow sublimation is a much larger mass sink than drifting snow transport over the whole ice sheet (Palm et al., 2017; Lenaerts et al.,2012a) but is still poorly constrained because observations are very scarce bellow 2000 m a.s.l. where it occurs."

- P12 L31: I am not aware that "dynamical downscaling of ERA-interim with RACO2 and MAR" is described above (or what do you want to say with "dynamical downscaling"?). Revise. And cite key figures supporting this sentence. **[corrected]**

"dynamical downscaling" is another term for "regional climate modelling", I replaced it by the second one, more usually used .

- P13 Fig. 5c: why do you define the difference as RACMO2 – MAR for this panel, though all the other three defines the difference as MAR-RACMO2. If you don't have a good reason, please use the same definition MAR-RACMO2 for all panels.

I changed for MAR-RACMO2 in panel c). The reason was that sublimation is a negative contribution to SMB and precipitation, so mapping RACMO2 - MAR for sublimation allows to directly compare the contribution of sublimation to SMB and ground precipitation shown in a) and b). But finally I agree it is clearer to plot MAR-RACMO2 everywhere.

- P13L2: In this study -> "In that study" or "In Grazioi et al (2017)" **[corrected]**
- P14L14: change to "2000 m a.s.l." **[corrected]**
- P14L27: change to "Figs. 5b and 5d" **[corrected]**
- P15 Fig. 6 y axis labels: unit for panels b and c are wrong. m-2, not m2.**[corrected]**
- P15 Fig.6 caption: line 2 from the top, change to "Figs. 5b and 5d". **[corrected]**
- I think both models use the same BEDAMP2 ice topography. So, why is the surface elevation different (apparent for 1700 km from B1)?

RACMO2 uses Bamber (2009) whereas MAR uses Bedmap2 (Fretwell et al., 2013). We added this information in the model description, and we also discuss it in the conclusion as you suggest bellow.

- Add unit for the curvature (0.005 and -0.005). **[corrected]**
- P16L5: again what does “dynamical downscaling” mean? Do you mean individual components of the climate models enforced by these reanalysis data? **[corrected]**
- P16L17: it is first time for me to see that the RACMO2 underestimates the drifting snow transport by a factor of three. It was not quantified earlier, and the factor of three suddenly appears in the conclusions and then abstract. In my opinion, Figure 4 cited here does not immediately support this statement. Please explain.

This statement is based on Section 3.2 (P12 L14-17 of first revised manuscript) :

"In Figure 4b, we propose a spatial estimate of the drifting snow transport fluxes not resolved by MAR, computed as a simple function of curvature and wind speed as described above. This estimate is comparable to the drifting snow transport pattern modelled by RACMO2 (Fig. 4c), except that it gives fluxes approximately three times larger than in RACMO2 (see differences in colour map scales between Fig. 4b and 4c, fluxes summed over the ice sheet and associated uncertainties are detailed in Table S2). "

This section is now more detailed :

"We propose that drifting snow transport fluxes (ds_{tr}) not resolved by MAR can be estimated as a scaling of curvature depending of wind speed: $ds_{tr} = \alpha(ws_{10}) \cdot$ curvature (Figure 4b). The scaling factor $\alpha(ws_{10})$ depends on wind thresholds to simulate the transition between no drifting snow transport for low wind speed ($\alpha = 0$ for $ws_{10} < 5$ m s^{-1}) and drifting snow transport scaled to curvature for high wind speed ($\alpha = 3700\ 10^6$ kg m^{-1} yr^{-1} for $ws_{10} > 9$ m s^{-1}), with a linearly increasing scaling factor between 5 and 9 m s^{-1} for a smooth transition around the 7 m s^{-1} wind threshold defined above. That estimate of drifting snow transport fluxes shows little sensitivity to the choice of the wind thresholds and of the scaling factor (see fluxes summed over the ice sheet for different thresholds and scaling factors in Table S2). The spatial pattern of drifting snow transport we obtain is comparable to the one simulated by RACMO2 (Fig. 4c), except that it gives fluxes more than three times larger than in RACMO2 (see Table S2, and note the different colour map scales between Fig. 4b and 4c)."

- P16L24-25: Revise.

We revised the sentence for the following:

"We also point out that MAR generally simulates larger SMB and snowfall amounts than RACMO2 inland, particularly on the lee side of the Transantarctic Mountains and on crests at the ice sheet margins, whereas MAR simulates lower snowfall than RACMO2 windward of mountain ranges and promontories."

- P16-17: I agree with the authors on the recommendations of future modeling work. Sublimation and thus wind speed should be better modeled for low elevated regions near the coast, where the surface topography is highly variable and BEDMAP2 topography is not accurate enough. So, model cell size and input topography data should be considered as well. Just a comment.

We added the following sentence at the end: *"The accuracy of the topography has to be considered as well, as digital elevation models are in constant improvement over the Antarctic ice sheet (e.g. Slater et al., 2018) and should be regularly updated in climate models."*

Editorial points in the supplement

We moved Fig.S13 to Fig.S5 according to its first citation in the manuscript, and we changed all the following numbering throughout the manuscript and supplement.

- Table S1 caption: unclear. Please revise what each number means. I think that the second number shows the number of model cells where the data are present for the specific depth range, and the first number shows the number of observations in total. For example, for 0-100 cm of Albert et al. (2007), only 1 cell has the observation data, and this cell has three data points.

Yes you are right. We changed the caption for the following: "*References of snow density datasets. For each depth range, we give the total number of observations (left) and the number of 35x35 km model grid cells they cover (right).*"

- Figure S1 caption: Table S1, not S2. **[corrected]**
- Figures S5 and S6 **[now S6 and S7]**: revise the unit to kg m-2 yr-1 in each panel. **[corrected, and also for S11…]**
- Figure S6 **[now S7]** caption: Table 2, not 1. **[corrected]**
- Figure S9 **[now S10]** caption: contour lines -> outlines. **[corrected]**
- Add a brief explanation why these data were excluded. Are they excluded because of the slow wind speed (< 7 m/s)?

The 2 excluded dots where excluded because they where outliers, and the 6 squares because of the low wind speed at those locations. I clarified this in the legend.

- Again, why do you use this 7-m/s criteria, though the regression is made for the locations where wind speed is more than 9 m/s? (it may be a typo, however).

This is the same explanation as above : we chose the 5/9 m s-1 thresholds to have a smooth transition around the 7 m s-1 threshold.

- Figure S10 **[now S11]**: the definition of positive and negative wind deflection is not clear. Is it better to define as eastward or westward?

It is defined this way because in Fig.3 we plot the variables against the distance along transect, from the coast (left) to the plateau (right). So the Coriolis deflection must be counted along this same axis : a deflection toward the coast shifts the wind backward in the axis (negative deflection), and a deflection toward the plateau shifts the wind upward in the axis (positive deflection). This information has been added to the legend.

- Figure S11 **[now S12]**: unit for the gas constant of water vapor should be J kg-1 K-1. Add "-1" after K. **[corrected]** Also thin normalized curves in Panels c and d are hardly readable. **[corrected]**
- Figure S11 **[now S12]**: Please add explanations for 95% and 99% envelopes.

In the caption it is said: *"The thick blue dashed line shows the 95% end of the distributions, and the thick blue solid line is the 99% end of the distributions."*

- Figure S12 **[now S13]**: check the very end of the caption. The curvature for the valleys must be wrong. **[corrected]**

Estimation of the Antarctic surface mass balance using the regional climate model MAR (1979-2015) and identification of dominant processes

Cécile Agosta[1,2,3], Charles Amory[1], Christoph Kittel[1], Anais Orsi[2], Vincent Favier[3], Hubert Gallée[3], Michiel R. van den Broeke[4], Jan T. M. Lenaerts[4,5], Jan Melchior van Wessem[4], Willem Jan van de Berg[4], and Xavier Fettweis[1]

[1]F.R.S.-FNRS, Laboratory of Climatology, Department of Geography, University of Liège, B-4000 Liège, Belgium
[2]Laboratoire des Sciences du Climat et de l'Environnement (IPSL/CEA-CNRS-UVSQ UMR 8212), CEA Saclay, F-91190 Gif-sur-Yvette, France
[3]Université Grenoble Alpes, CNRS, Institut des Géosciences de l'Environnement, F-38000, Grenoble,France
[4]Institute for Marine and Atmospheric Research Utrecht, Utrecht University, Utrecht, the Netherlands
[5]Department of Atmospheric and Oceanic Sciences, University of Colorado Boulder, Boulder CO, United States of America

Correspondence: Cécile Agosta (cecile.agosta@gmail.com)

Abstract. The Antarctic ice sheet mass balance is a major component of the sea level budget and results from the difference of two fluxes of a similar magnitude: ice flow discharging in the ocean and net snow accumulation on the ice sheet surface, i.e. the surface mass balance (SMB). Separately modelling ice dynamics and surface mass balance is the only way to project future trends. In addition, mass balance studies frequently use regional climate models (RCMs) outputs as an alternative to observed fields because SMB observations are particularly scarce on the ice sheet. Here we evaluate new simulations of the polar RCM MAR forced by three reanalyses, ERA-Interim, JRA-55 and MERRA2, for the period 1979-2015, and we compare MAR results to the last outputs of the RCM RACMO2 forced by ERA-Interim. We show that MAR and RACMO2 perform similarly well in simulating coast to plateau SMB gradients, and we find no significant differences in their simulated SMB when integrated over the ice sheet or its major basins. More importantly, we outline and quantify missing or underestimated processes in both RCMs. Along stake transects, we show that both models accumulate too much snow on crests, and not enough snow in valleys, as a result of drifting snow transport fluxes not included in MAR and probably underestimated in RACMO2 by a factor of three. Our results tend to confirm that drifting snow transport and sublimation fluxes are much larger than previous model-based estimates and need to be better resolved and constrained in climate models. ~~MAR generally simulates larger SMB and snowfall amounts than RACMO2 inland, particularly on the lee side of topographic barriers, whereas lower snowfall amounts are found windward of topographic barriers and in valleys at the ice sheet margins.~~ Sublimation of precipitating particles in low-level atmospheric layers is ~~largely~~ responsible for the significantly lower snowfall rates in MAR than in RACMO2 in katabatic channels at the ice sheet margins. Atmospheric sublimation in MAR represents 363 $\mathrm{Gt\ yr^{-1}}$ over the grounded ice sheet for the year 2015, which is 16 % of the simulated snowfall loaded at the ground. This estimate is consistent with a recent study based on precipitation radar observations, and is more than twice as much as simulated in RACMO2, because of different time residence of precipitating particles in the atmosphere. The remaining spatial differences in snowfall between MAR and

RACMO2 are attributed to differences in advection of precipitation, snowfall particles being likely advected too far inland in MAR.

1 Introduction

Mass loss from the Antarctic ice sheet (AIS) and therewith its contribution to the sea level budget results from the difference of two fluxes of a similar magnitude: ice flow discharging in the ocean (D) and net snow accumulation on the ice sheet surface, i.e. the surface mass balance (SMB). The total ice sheet mass balance (SMB minus D) can be assessed using satellite altimetry, gravimetry or the input–output method (Shepherd et al., 2018), which all request surface mass balance estimates. The input-output method, which consists in separately modelling ice dynamics and surface mass balance, is also the only way to project future trends.

Surface mass balance as used in this study is the sum of mass gains (mainly snowfall accumulation and some riming), mass losses (mainly surface and drifting snow sublimation, some liquid water runoff) and drifting snow transport (defined as the horizontal advection of the drifting snow) which can lead to either mass gain or mass loss. Snowfall rates are one order of magnitude larger than all of the other SMB fluxes at the continental scale (Lenaerts et al., 2012b), with the largest amounts found along the ice sheet margins due to cyclonic activity in the Southern Ocean and to the orographic lifting of relatively warm and moist air masses (van Wessem et al., 2014; Favier et al., 2017). Accumulation patterns are highly variable at the kilometre scale and from year to year (e.g., Agosta et al., 2012). Consequently, proper observations of SMB require a high spatial coverage (e.g. stake-lines, accumulation radars plus ice-cores for layer dating and snow density) and a temporal sampling spanning several years (Eisen et al., 2008). Even if efforts have been made to fulfil those requirements, ground-based observations are scarce and carry with them high logistical costs in this cold, windy and remote environment. Interpolation techniques used to interpolate the scarce SMB observations (Vaughan et al., 1999; Arthern et al., 2006) encounter major caveats (Magand et al., 2008; Genthon et al., 2009; Picard et al., 2009).

This is why many AIS mass balance studies use output of regional climate models (RCMs) to estimate ice sheet SMB for the recent decades (e.g., Rignot et al., 2011; Gardner et al., 2018; Shepherd et al., 2018). In order to obtain a good agreement with observations, atmospheric models require accurate large-scale circulation patterns together with a proper representation of snow surface processes, clouds, turbulent fluxes, and a relatively high horizontal resolution to properly resolve the complex ice sheet topography at the margins.

Here, we present new simulations of the regional climate model MAR, applied for the first time over the whole AIS, but already widely used for polar studies, e.g. in Greenland (Fettweis et al., 2013, 2017), Svalbard (Lang et al., 2015), Adélie Land (Antarctic coastal area, Gallée et al., 2013; Amory et al., 2015) and Dome C (Antarctic plateau, Gallée et al., 2015). We compare MAR-simulated SMB with the state-of-the-art regional climate model RACMO2 (van Wessem et al., 2018). We use available SMB observational datasets to show that MAR and RACMO2 perform similarly well in simulating the SMB spatial gradients. In addition, we identify significant processes that still need to be included or improved in both RCMs.

In Section 2, we describe MAR and its specific set-up for Antarctica, together with RACMO2, the forcing fields, observational datasets and methods designed for model evaluation. In Section 3, we show that both RCMs share common biases against observed SMB, resulting from drifting snow transport fluxes. Secondly, we analyse SMB differences between models and show that many of the discrepancies can be attributed to low-level sublimation of precipitation in katabatic channels and to the difference in precipitation advection inland. Finally, in Section 4, we summarise our main findings and discuss further efforts to be achieved for a better assessment of the AIS surface mass balance.

2 Data and methods

2.1 Regional modelling

2.1.1 Regional atmospheric models

For the first time, the polar-oriented regional atmospheric model MAR is applied for decades-long simulations over the whole Antarctic ice sheet. MAR atmospheric dynamics are based on the hydrostatic approximation of the primitive equations, fully described in Gallée and Schayes (1994). Prognostic equations are used to depict five water species: specific humidity, cloud droplets and ice crystals, raindrops and snow particles (Gallée, 1995). Sublimation of airborne snow particles is a direct contribution to the heat and moisture budget of the atmospheric layer in which these particles are simulated. The radiative transfer through the atmosphere is parametrised as in Morcrette (2002), with snow particles affecting the atmospheric optical depth (Gallée and Gorodetskaya, 2010). The atmospheric component is coupled to the surface scheme SISVAT (soil ice snow vegetation atmosphere transfer, De Ridder and Gallée, 1998) dealing with the energy and mass exchanges between surface, snow and atmosphere. The snow–ice part of SISVAT is based on the snow model CROCUS (Brun et al., 1992). It is a one-dimensional multilayered energy balance model which simulates meltwater refreezing, snow metamorphism and snow surface albedo depending on snow properties. We used MAR version 3.6.4, simply called MAR here-after. In this version the physical settings are the same as in MAR version 3.5.2 used for Greenland (Fettweis et al., 2017), except for the adaptations detailed below.

Grid: Projection is the standard Antarctic polar stereographic (EPSG:3031). The horizontal resolution is 35 km, an intermediate resolution that results from a computation time compromise in order to run the model with multiple reanalyses and global climate model forcings over the 20th and the 21st century. The vertical discretisation is composed of 23 hybrid levels from $\sim$2 m to $\sim$17000 m above the ground.

Boundaries: The topography is derived from the Bedmap2 surface elevation dataset (Fretwell et al., 2013). Because the Antarctic domain is about 4 times larger than the Greenland domain, the circulation has to be more strongly constrained. This is why we use a boundary relaxation of temperature and wind in the upper atmosphere starting from 400 hPa ($\sim$6000 m above the ground) to 50 hPa (upper level), as in van de Berg and Medley (2016), whereas relaxation starts from 200 hPa in Fettweis et al. (2017).

Parameterisations:

a) The surface snow density ρ_s (kg m^{-3}) is computed as a function of 10 m wind speed ws_{10} (m s^{-1}) and surface temperature T_s (K):

$$\rho_s = 149.2 + 6.84\, ws_{10} + 0.48\, T_s, \quad (1)$$

with minimum-maximum values of 200–400 kg m^{-3}. This parameterisation was defined so that the simulated density of the first 50 cm of snow fits observations collected over the Antarctic ice sheet (see Fig. S1, with snow density database detailed in Table S1).

b) The aerodynamic roughness length z_0 is computed as a function of the air temperature, as proposed in Amory et al. (2017). The parameterisation was tuned so that z_0 fit the observed seasonal variation between high (> 1 mm) summer and lower (0.1 mm) winter values in coastal Adélie Land, for air temperatures above -20 °C. For lower temperatures, z_0 is kept constant and set to 0.2 mm, in agreement with observed z_0 values on the Antarctic Plateau (e.g., Vignon et al., 2016);

c) As in Fettweis et al. (2017), the MAR drifting snow scheme is not activated, because this scheme was sensitive to parameter choices (Amory et al., 2015). An updated version of the drifting snow scheme is currently being developed and evaluated for application at the scale of the whole ice sheet.

We compare MAR results over the AIS to the latest outputs of the regional atmospheric model RACMO2 version 2.3p2 (van Wessem et al., 2018), called RACMO2 here-after, using a horizontal resolution of 27 km~~and~~, a vertical resolution of 40 atmospheric levels, and a topography based on the digital elevation model from Bamber et al. (2009). This regional model is developed by the Royal Netherlands Meteorological Institute (KNMI), and has subsequently been adapted for modelling the Antarctic climate and its surface mass balance (van de Berg et al., 2006). It includes a drifting snow scheme (Lenaerts et al., 2012a), an albedo routine with prognostic snow grain size (Kuipers Munneke et al., 2011), and a multilayer snow model computing melt, percolation, refreezing and runoff (Ettema et al., 2010).

MAR and RACMO2 models were developed independently. We will not detail here the many physical parameterisation differences between both RCMs, but we will later highlight some of them we show having a significant impact on the modelled SMB.

2.1.2 Forcing reanalyses

Regional atmospheric models are forced by atmospheric fields at their lateral boundaries (pressure, wind, temperature, humidity), at the top of the troposphere (temperature, wind), as well as by sea surface conditions (sea ice concentration, sea surface temperature) every six hours. Consequently, regional atmospheric models add details and physics to the forcing model in the mid and lower troposphere and at the land or iced surface, whereas large-scale circulation patterns are driven by the forcing fields. We forced MAR with three reanalyses over Antarctica in order to evaluate the uncertainty in the simulated surface climate arising from the uncertainty in the assimilation systems: the European Centre for Medium-Range Weather Forecasts "Interim" re-analysis (here-after ERA-Interim, resolution ∼0.75°, i.e. ∼50 km at 70 °S, Dee et al., 2011), the Modern-Era

Retrospective analysis for Research and Applications Version 2 (here-after MERRA2, resolution ∼0.5°, Gelaro et al., 2017), and the Japanese 55-year Reanalysis from the Japan Meteorological Agency (here-after JRA-55, resolution ∼1.25°, Kobayashi et al., 2015).

The regional atmospheric model RACMO2 is forced by ERA-Interim. We focus our study to the period 1979-2015, as reanalyses are known to be unreliable before 1979, when satellite sounding data started to be assimilated (Bromwich et al., 2007).

2.2 Observations

2.2.1 SMB observations and sectors of strong SMB gradients

We use surface mass balance observations of the GLACIOCLIM-SAMBA dataset detailed in Favier et al. (2013) and updated by Wang et al. (2016). This dataset is an update of the one assembled by Vaughan et al. (1999) following the quality-control methodology defined by Magand et al. (2007). It includes 3043 reliable SMB values averaged over more than 3 years. We add accumulation estimates from Medley et al. (2014), retrieved over the Amundsen Sea coast (Marie Byrd Land) with an airborne-radar method combined with ice-core glaciochemical analysis.

The first order feature of the Antarctic SMB is a strong coastal-inland gradient, with mean values ranging from typically greater than 500 $\mathrm{kg\,m^{-2}\,yr^{-1}}$ at the ice sheet margins to about 30 $\mathrm{kg\,m^{-2}\,yr^{-1}}$ in the dry interior plateau ~~(Fig. 1, see also, e.g., Wang et al., . We divide the sparse observation dataset (Fig. 1 –~~ (Fig. 1a, see also, e.g., Wang et al., 2016). As observations only cover 5 % of MAR grid cells ~~coverage of~~ over the ice sheet~~)~~, we divide that sparse observation dataset into 10 sectors detailed in Table 1 and shown in Fig. 2. Six of them are stake transects with a stake every ∼1.5 km, which have been proven very valuable for evaluating modelled SMB (Agosta et al., 2012; Favier et al., 2013; Wang et al., 2016). The four other sectors are composed of more scattered observations covering large elevation ranges (Victoria Land, Dronning Maud Land, and Ross Ice Shelf–Marie Byrd Land).

2.2.2 Model-observation comparison method

RACMO2 outputs are bi-linearly interpolated to the 35×35 km MAR grid. For each SMB observation, we consider the 4 surrounding MAR grid cells, from which we eliminate ocean grid cells. We also eliminate surrounding grid cells with an elevation difference with the observation greater than 200 m (missing elevation of observation is set to Bedmap2 elevation at 1 km resolution). Finally, we bi-linearly interpolate model values of the remaining grid cells at the observation location (see schematic in Fig. S2).

As we restrict our modelling study to the 1979-2015 period, we only consider observations beginning after 1950. For observations beginning after 1979, we time-average model outputs for the same period as the observation. We keep observations beginning before 1979 only if they cover more than eight years, and in this case we compare the observed value with the modelled value time-averaged for 1979-2015.

Table 1. Sectors extracted from the GLACIOCLIM-SAMBA database.

Sector name	Sector type	Nb. of obs.	Nb. of grid cells	Year range	Elevation range (~~m~~ m a.s.l.)	Ref.
Marie Byrd Land	Radar transects	6615	57	1980–2009	973–1873	[1]
Ross–Marie Byrd Land	Scattered	72	51	1950–1991	37–1995	[2,3,4]
Victoria Land	Scattered	60	40	1951–2006	1804–3240	[5,6,7]
Dumont-d'Urville–Dome C	Transect	116	24	1955–2010	633–3240	[5,8,9,10]
Law Dome–Wilkes Land	Transect	382	32	1973–1986	801–2232	[11]
Zhongshan–Dome A	Transect	583	40	1994–2011	1031–4081	[12,13]
Mawson–Lambert Glacier	Transect	515	36	1990–1995	1883–2924	[14]
Syowa–Dome F	Transect	507	38	1955–2010	584–3803	[15]
Princ. Elisabeth	Transect	58	6	2009–2012	47–1071	[16]
Dronning Maud Land	Scattered	376	104	1955–2008	1753–3741	[17,18,19,20]

[1] Medley et al. (2014), [2] Clausen et al. (1979), [3] Venteris and Whillans (1998), [4] Vaughan et al. (1999), [5] Magand et al. (2007), [6] Frezzotti et al. (2004), [7] Frezzotti et al. (2007), [8] Pettré et al. (1986), [9] Agosta et al. (2012), [10] Verfaillie et al. (2012), [11] Goodwin (1988), [12] Ding et al. (2011), [13] Wang et al. (2016), [14] Higham and Craven (1997), [15] Wang et al. (2015), [16] GLACIOCLIM-BELARE, [17] Picciotto et al. (1968), [18] Mosley-Thompson et al. (1995), [19] Mosley-Thompson et al. (1999), [20] Anschütz et al. (2011).

In a last step, we average-out the kilometre-scale variability of the observed SMB (Agosta et al., 2012) by binning point values onto grid cells. For each grid cell containing multiple observations, we average all observations contained into the grid cell weighted by the time span of observations, and in the same way we weight-average the modelled values interpolated to observation locations. This way, we obtain consistent observed and modelled averaged values on grid cells.

We discard 66 observations beginning before 1979 and spanning less than eight years. We also discard 12 observations for which the four surrounding grid cells fall in ocean, and seven observations located at specific topographic features for which none of the four surrounding grid cell has an elevation difference less than 200 m with respect to the actual location. After this, we retain 559 model-observation comparisons.

3 Results

3.1 Evaluation of the modelled SMB

The large spatial Antarctic SMB gradients, shown in Fig. 1a as modelled by MAR forced by ERA-Interim for the period 1979-2015, coincide with a strong interannual variability (Fig. 1b), expressed by a standard deviation of ~22% of the mean SMB on average over the ice sheet (Fig. 1c). MAR SMB shows no systematic spatial bias (Fig. 1d), with a mean bias of 6 $\mathrm{kg\ m^{-2}\ yr^{-1}}$ (4% of the mean observed SMB), as well as a very strong correlation with the observed SMB (R^2=0.83, p-value<0.01,

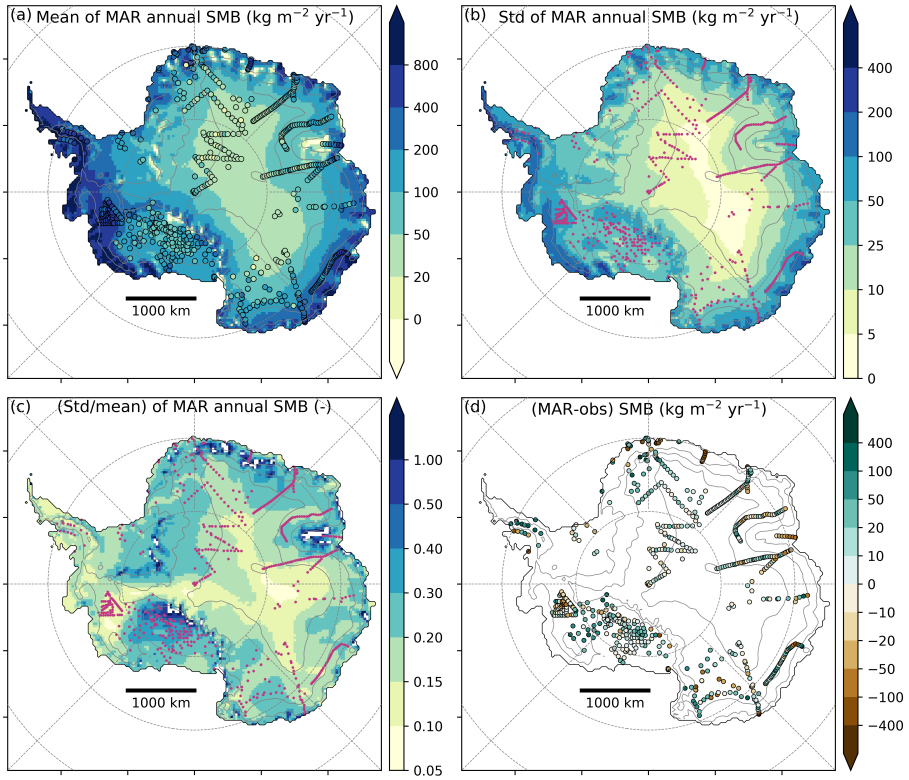

Figure 1. MAR SMB for the period 1979-2015: (a) mean annual SMB, with coloured dots showing the observed SMB values (shared colour scale); (b) standard deviation of annual SMB; (c) standard deviation divided by mean annual SMB; (d) difference between MAR and observed SMB on MAR grid cells, following the methodology detailed in Section 2.2.2. Magenta dots in panels b) and c) show the location of SMB observations. Solid grey lines are contours of surface height every 1000 m above sea level. Latitude circles are -60°S, -70°S and -80°S, and longitude lines are from 145°W to 145°E by step of 45°.

computed on the logarithm of SMB values, as SMB distributions are log-normal). RACMO2 shows similar performance (mean bias of -3 kg m^{-2} yr^{-1}, R^2=0.86, computed on the logarithm of SMB as well).

The model-observation comparison by sectors (Fig. 2) reveals a good representation of the coast-to-plateau SMB gradients by both RCMs. MAR and RACMO2 are in good agreement despite MAR not including drifting snow processes whereas RACMO2 does, except in Ross–Marie Byrd Land and in Victoria Land where MAR simulates larger SMB than RACMO2. Another noticeable result is that MAR forced by ERA-Interim, JRA-55 and MERRA2 give very similar results for the SMB spatial pattern, not only at the observation locations (Fig. 2) but also at the ice sheet scale (comparisons of MAR SMB for different forcing reanalyses are shown in Fig. S4, ~~note the colour map scales compared to~~ with colormap scales 10 time smaller than in Fig. ~~S9~~S5 where MAR is compared to RACMO2). This is why we focus on MAR forced by ERA-Interim in the following.

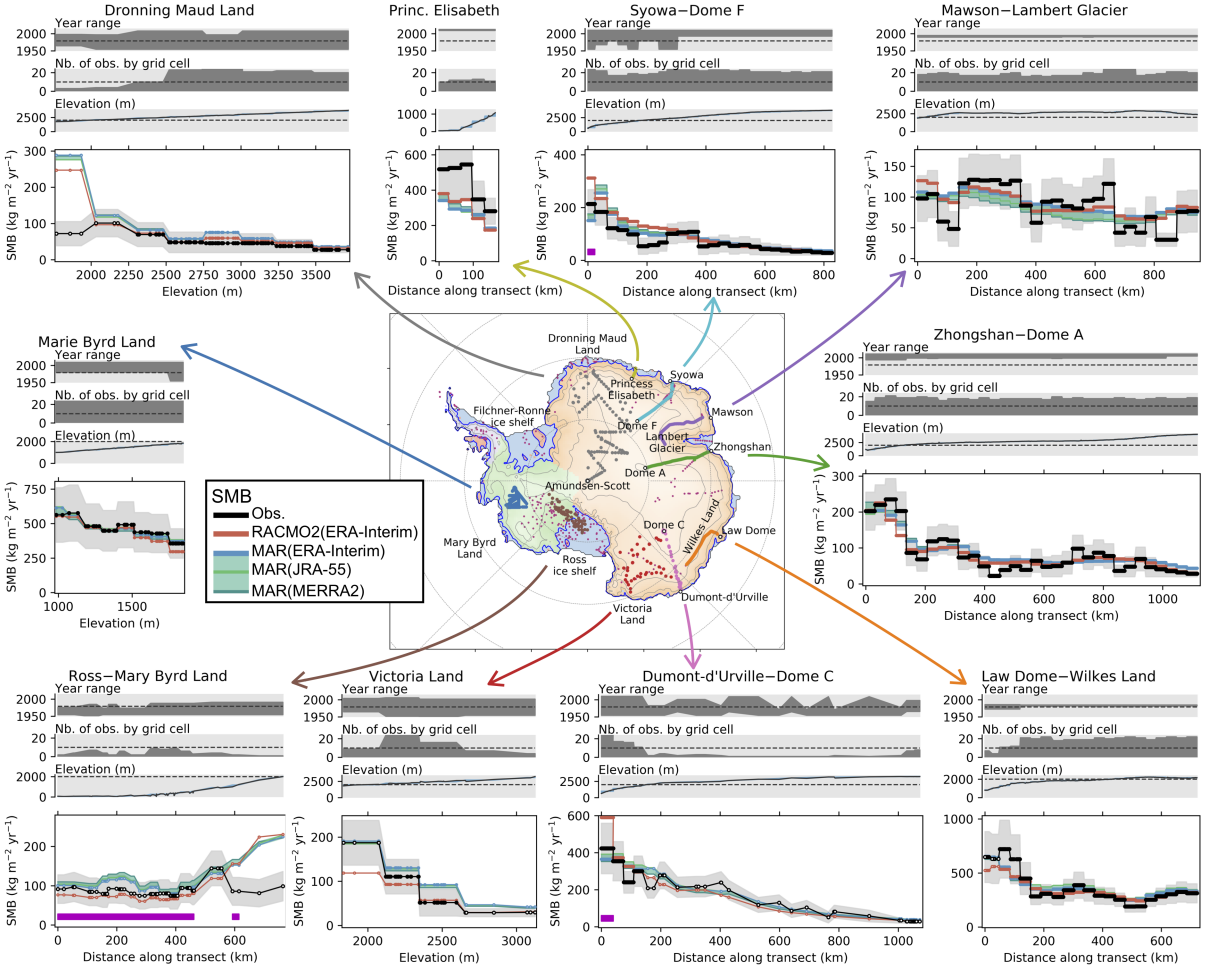

Figure 2. Modelled vs. observed SMB for sectors and transects as detailed in Table 1. RACMO2 outputs are bi-linearly interpolated to the MAR grid. SMB values are first averaged on MAR grid cells (Sec. 2.2.2) then along chosen grid direction (Fig. S2) or by elevation bins. Distance along transect starts at the coast. Uncertainty of observed SMB (grey shaded area) is the standard deviation of observations contained in each grid cell (sub-grid variability), estimated as a function of the mean observed SMB (see Fig. S3). Despite SMB values corresponding to grid cell averages, we display one marker for each observation, with the x axis corresponding to the observation location along transect or elevation. ~~Markers~~ For observed SMB plots, markers with white faces are for bins containing less than 10 observations and black faces for bins containing more than 10 observations. Magenta bands mark grid cells where more than 15 % of precipitation sublimates in the katabatic layers according to Grazioli et al. (2017). The map shows the main Antarctic basins: Antarctic Peninsula in purple, West Antarctic ice sheet in green, and East Antarctic ice sheet in orange. Ice shelves are mapped in blue, grounded islands in red, and the blue line shows the location of the grounding line.

We find no significant differences in the SMB simulated by MAR and RACMO2 when integrated over the ice sheet or its major basins (Table 2). SMB is driven by snowfall amounts, which are more than 10 times larger than other SMB components.

Snow sublimation in RACMO2 is the sum of sublimation at the surface of the snowpack and of drifting snow sublimation, and is approximately 50 % larger than in MAR which only includes surface snow sublimation. However, surface snow sublimation alone is almost two times larger in MAR than in RACMO2 (Table 2 ~~, also~~ and spatial patterns shown in Fig. ~~S5~~S6), which we investigate in the next section. Modelled surface melt is less than half of the sublimation amount, however liquid water almost entirely refreezes into the snowpack in both models (maps of MAR and RACMO2 modelled melt amounts are shown in Fig. ~~S6~~S7). Temporal variability of the SMB and its components is fully driven in both RCMs by the forcing reanalyses and are therefore strongly correlated with each other (time series shown in Fig. ~~S7~~S8). We do not elaborate on the SMB temporal variability here as this aspect will be further detailed in a forthcoming study.

3.2 Drifting snow transport features

~~Fluctuations~~ Local fluctuations of the observed SMB around the smooth modelled SMB gradients are apparent along the four stake transects covering more than 500 km: Law Dome–Wilkes Land, Zhongshan–Dome A, Mawson–Lambert Glacier, and Syowa–Dome F. We related these fluctuations to drifting snow transport. Indeed, the snow eroded from the snowpack is loaded into the atmosphere, where it can sublimate and be transported by the wind. Katabatic winds blowing on the surface of the ice sheet result from the downslope gravity flow of cold, dense air. As a consequence, the surface wind divergence, which drives the snowdrift mass transport, is strongly related to the curvature of the topography~~(see~~ , and both have similar spatial patterns (shown in Fig. ~~S8):~~ S9). This is because slopes becoming steeper (crests, positive curvature) will lead to wind speed acceleration (positive wind divergence), thus to drifting snow export (mass loss), whereas slopes becoming more gentle (valleys, negative curvature) will lead to wind speed deceleration (negative wind divergence), thus to drifting snow deposit (mass gain).

To test our hypothesis, we computed the mean curvature of the MAR 35×35 km elevation field. In Fig. 3, we notice that both RCMs commonly exhibit an excess of accumulation on crests and a deficit of accumulation in valleys, in the range of ± 40 kg m^{-2} yr^{-1}. To quantify this curvature effect, we correlate MAR SMB bias (ΔSMB) with the curvature. For each transect, we apply a constant shift of $\pm$ one grid cell to the curvature in order to find the maximum correlation with ΔSMB~~(~~. For three out of the four transects, we find only one shift for which the correlation is significant, and for remaining transect (Syowa–Dome F) we find no significant correlation (Fig. ~~S9~~S10). The sign and the amplitude of ~~these~~ those shifts are in line with curvature being used as a proxy for wind divergence, as they are consistent with the Coriolis wind deflection westward of the topography gradient (detailed in Fig. ~~S10). When the mean annual 10 wind speed (ws_{10}) is greater than seven ,~~ S11). After applying those shifts, we find that the difference between modelled and observed SMB (in kg m^{-2} yr^{-1}) is scaled to approximately 3700 ± 1100 (in 10^6 kg m^{-1} yr^{-1}) times the curvature (in 10^{-6} m^{-1}), with a significant relationship (R^2 = 0.41, Fig. 4a), when the mean annual 10 m wind speed (ws_{10}) is greater than seven m s^{-1}. For lower wind speed ($ws_{10} < 7$ m s^{-1}), we no longer observe any relationship between model bias in SMB and curvature (horizontally aligned squares in Fig. 4a). This is consistent with the drifting snow transport process which requires the wind speed to reach threshold values for the erosion to be initiated (Amory et al., 2015).

Hence, a large part of the discrepancies between modelled and observed SMB is explained by ~~elevation~~ surface curvature when wind speed is sufficiently high, which we relate to the unresolved drifting snow transport in MAR. We are able to catch

Table 2. Antarctic integrated SMB on average for 1979-2015 ± one standard deviation of annual values, in $\mathrm{Gt\ yr^{-1}}$. Antarctic Ice Sheet (AIS) and basins geometry are based on Rignot basins (Shepherd et al., 2018), shown in Fig. 2. RACMO2 is bi-linearly interpolated on MAR grid and the same mask is applied to both models, with area given for this mask. SMB is computed as follows: MAR SMB = Snowfall + Rainfall − Surface snow sublimation − Run-off; RACMO2 SMB = Snowfall + Rainfall - Surface snow sublimation - Drifting snow sublimation - Drifting snow transport - Run-off.

Basin	Area (10^6 km^2)	Component ($\mathrm{Gt\ yr^{-1}}$)	MAR(ERA-Interim)	RACMO2(ERA-Interim)
Total AIS	13.41	SMB	2200 ± 115	2177 ± 107
w/o Peninsula		Snowfall	2306 ± 111	2339 ± 107
		Rainfall	6 ± 1	2 ± 1
		Surface snow sublimation	111 ± 10	57 ± 4
		Drifting snow sublimation	–	101 ± 5
		Drifting snow transport	–	5 ± 0
		Run-off	1 ± 1	1 ± 1
		Melt	40 ± 20	68 ± 30
Total AIS	13.83	SMB	2517 ± 111	2516 ± 105
Grounded AIS	12.04	SMB	1923 ± 100	1857 ± 94
w/o Peninsula		Snowfall	1995 ± 97	1987 ± 94
		Surface snow sublimation	77 ± 8	39 ± 3
		Drifting snow sublimation	–	87 ± 4
Grounded AIS	12.27	SMB	2120 ± 99	2068 ± 93
Grounded East AIS	9.77	SMB	1170 ± 89	1121 ± 80
		Snowfall	1245 ± 87	1225 ± 82
		Surface snow sublimation	77 ± 6	34 ± 3
		Drifting snow sublimation	–	66 ± 4
Grounded West AIS	2.11	SMB	675 ± 62	643 ± 62
		Snowfall	675 ± 61	668 ± 62
		Surface snow sublimation	1 ± 3	4 ± 1
		Drifting snow sublimation	–	20 ± 2
Grounded Islands	0.16	SMB	78 ± 7	93 ± 8
Grounded Peninsula	0.23	SMB	198 ± 26	211 ± 27

the drifting snow transport signal because drifting snow sublimation is negligible for the four studied transects, as they are located at high elevation~~(>~~, upper than 2000 ~~m~~ m above sea level ~~– asl~~(a.s.l.), where the cold atmosphere has low capacity to

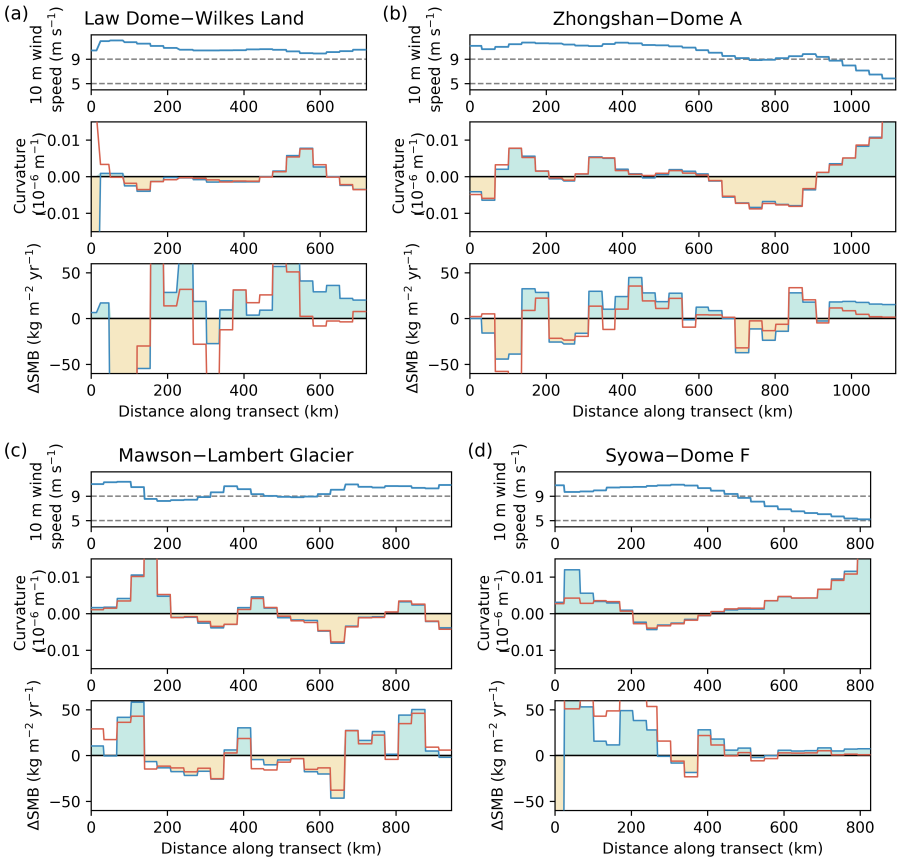

Figure 3. For each transect, we show (top) annual mean 10 m wind speed, (middle) curvature of elevation and (bottom) ~~difference in~~ modelled SMB ~~between models and observation~~minus observed SMB. Blue lines and colour shading are for MAR(ERA-Interim) outputs and red lines are for RACMO2(ERA-Interim) outputs. Values are computed as in Fig. 2. For Law Dome–Wilkes Land, MAR SMB is shifted by -30 kg m^{-2} yr^{-1}.

be loaded with moisture (see detailed analysis in Fig. ~~S11~~S12). The moisture holding capacity of the atmospheric boundary layer is an upper bound for drifting snow sublimation and quickly tends to zero when the mean air temperature decreases below -30°C, which is the case along most of the transects, whereas the amplitude of observed SMB fluctuations around the smooth SMB gradient is independent of the temperature (Fig. ~~S12~~S13).

~~In Figure 4b~~Consequently, we propose ~~a spatial estimate of the~~ that drifting snow transport fluxes (ds_{tr}) not resolved by MAR ~~, computed as a simple function of curvature~~ can be estimated as a scaling of curvature depending of wind speed: $ds_{tr} = \alpha(ws_{10}) \cdot curvature$ (Figure 4b). The scaling factor $\alpha(ws_{10})$ depends on wind thresholds to simulate the transition between no drifting snow transport for low wind speed ($\alpha = 0$ for $ws_{10} < 5$ m s^{-1}) and drifting snow transport scaled to curvature for high wind speed ($\alpha = 3700$ 10^6 kg m^{-1} yr^{-1} for $ws_{10} > 9$ m s^{-1}), with a linearly increasing scaling factor between 5 and ~~wind speed as described above. This estimate is comparable to the~~ 9 m s^{-1} for a smooth transition around the

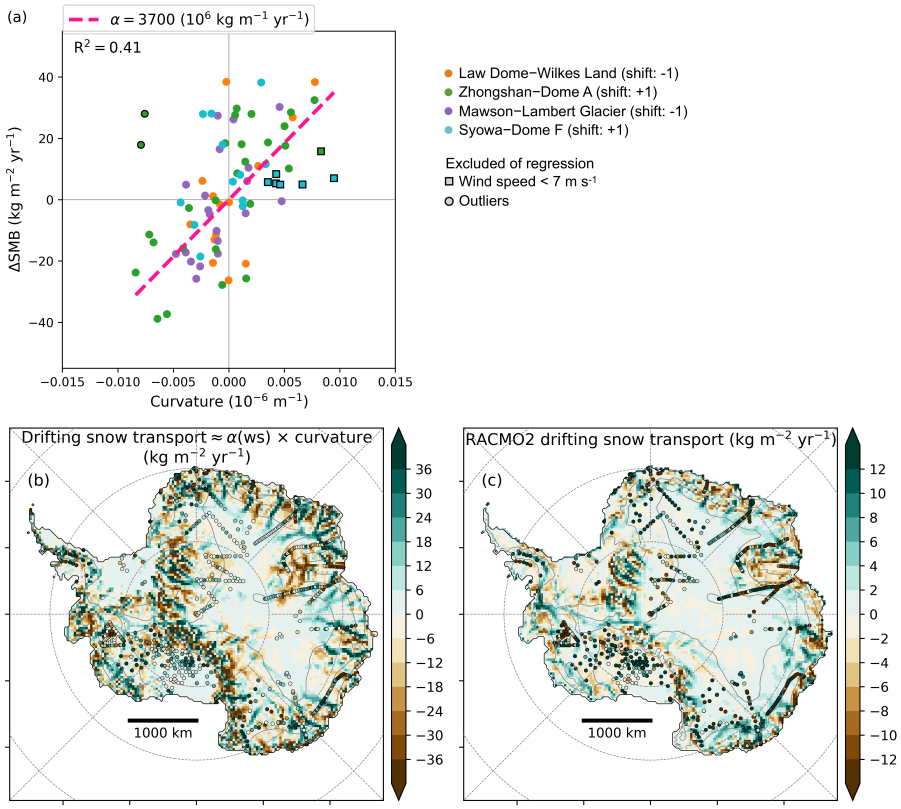

Figure 4. (a) Difference in SMB by grid cell (ΔSMB) between MAR(ERA-Interim) and observations for four transects (Law Dome–Wilkes Land, Zhongshan–Dome A, Mawson–Lambert Glacier, and Syowa–Dome F) vs. ~~elevation~~ surface curvature on MAR grid. Curvature is shifted by ± 1 grid cell according to the maximum correlation with ΔSMB (Fig. ~~S8~~S9). Linear regression through the origin is plotted with a dashed pink line. We excluded of regression two outliers (dots with black ~~contour~~outlines) and seven data for which MAR annual 10 m wind speed is lower than 7 m s^{-1} (squares with black ~~contour~~outlines). (b) Estimate of mean annual drifting snow transport based on a scaling of the curvature: drifting snow transport (~~kg m^{-2} yr^{-1}~~kg m^{-2} yr^{-1}) = α (~~10^6 kg m^{-1} yr^{-1}~~10^6 kg m^{-1} yr^{-1}) × curvature (~~10^{-6} m^{-1}~~10^{-6} m^{-1}), with $\alpha = 0$ ~~kg m^{-1} yr^{-1}~~kg m^{-1} yr^{-1} for wind speed lower than 5 ~~m s^{-1}~~m s^{-1}, $\alpha = 3700$ ~~10^6 kg m^{-1} yr^{-1}~~10^6 kg m^{-1} yr^{-1} for wind speed greater than 9 ~~m s^{-1}~~m s^{-1}, and α linearly increasing as a function of wind speed in between, around the 7 m s^{-1} wind speed threshold. Wind speed is the annual mean of 10 m wind speed modelled by MAR(ERA-Interim). Coloured dots show the difference between MAR SMB and observed SMB with the same colour scale. (c) Mean annual drifting snow transport flux in RACMO2 on average for 1979-2015 (kg m^{-2} yr^{-1}). Coloured dots show the difference between MAR SMB and observed SMB with the same colour scale.

7 m s^{-1} wind threshold defined above. That estimate of drifting snow transport fluxes shows little sensitivity to the choice of the wind thresholds and of the scaling factor (see fluxes summed over the ice sheet for different thresholds and scaling factors in Table S2). The spatial pattern of drifting snow transport ~~pattern modelled~~ we obtain is comparable to the one simulated by RACMO2 (Fig. 4c), except that it gives fluxes ~~approximately~~ more than three times larger than in RACMO2 (~~see differences in~~ Table S2, and note the different colour map scales between Fig. 4b and 4c~~, fluxes summed over the ice sheet and associated~~

~~uncertainties are detailed in Table S2~~). The drifting snow transport estimate consists in a redistribution of mass with negligible net mass loss over the Antarctic ice sheet (total AIS mass gain of $\sim$75 Gt yr^{-1} and total AIS mass loss of $\sim$80 Gt yr^{-1}, see Table S2).

~~Drifting snow sublimation might be the largest mass sink in Antarctica, much larger than the~~ Our drifting snow transport ~~fluxes at the scale of the ice-sheet (Palm et al., 2017; Lenaerts et al., 2012a). However, we cannot constrain this flux with the available SMB observation dataset, as it occurs bellow~~ estimate gives a good constraint for drifting snow fluxes above 2000 ~~m asl (Fig. S11d), where observations are extremely scarce. Our~~ m a.s.l., where low temperatures induce negligible atmospheric sublimation. As drifting snow transport ~~estimate can be used to constrain the drifting snow fluxes in models above 2000 m asl, which might have in turn implication for the~~ is proportional to the amount of snow in suspension in the atmosphere, quantifying this flux also enables to constrain the amount of snow eroded from the snowpack to the atmosphere, which drives drifting snow sublimation ~~amounts simulated at the ice-sheet margins.~~fluxes at lower elevation. This is of importance as drifting snow sublimation is a much larger mass sink than drifting snow transport over the whole ice sheet (Palm et al., 2017; Lenaerts et al., 2012a) but is still poorly constrained because observations are very scarce bellow 2000 m a.s.l. where it occurs.

Drifting snow sublimation included in RACMO2 and not in MAR moisten the surface atmospheric layers, consequently reducing the sublimation at the surface of the snowpack. This might explains the stronger surface snow sublimation in MAR than in RACMO2 (Table 2 and Fig. ~~S5~~S6). However, drifting snow sublimation is a potentially larger mass sink than surface snow sublimation, as drifting snow particles are continuously ventilated and fully exposed to the ambient air. Consequently, by accounting for drifting snow in MAR we expect that the drifting snow sublimation mass sink could be enhanced at the expense of surface snow sublimation at the ice sheet margins.

3.3 Sublimation of precipitation in low-level atmosphere

As described above, ~~the dynamical downscaling of ERA-Interim with~~ MAR and RACMO2 ~~and MAR results in~~ regional climate models forced with ERA-Interim simulate similar spatial patterns for SMB as compared to observations ~~.~~(Fig. 2). However, at the ice sheet scale, MAR and RACMO2 SMB show regional discrepancies (shown in Fig. 5a for 2015, and similar than the 1979-2015 mean ~~,~~ shown in Fig. ~~S13a~~S5a) which are primarily the result of differences in simulated snowfall rates (Fig. 5b, and ~~S13b~~S5b). We notice that areas where MAR snowfall is much lower than RACMO2 snowfall (Fig. 5b, dashed blue lines) coincide almost exactly with the pattern of precipitation that is able to sublimate in the low-level atmosphere according to Grazioli et al. (2017). In ~~this~~ that study, the amount of atmospheric sublimation is quantified for the year 2015 using atmospheric modelling constrained with precipitation radar observations. Atmospheric sublimation happens because the katabatic surface air flux, moving from high-elevated inland plateau toward sea level, is subject to adiabatic compression when it moves downslope. This compression induces an increase in air temperature which reduces relative humidity and drives sublimation rates in the lower troposphere ($\sim$first 1000 m above the ground), enhanced in the katabatic channels at the ice sheet margins.

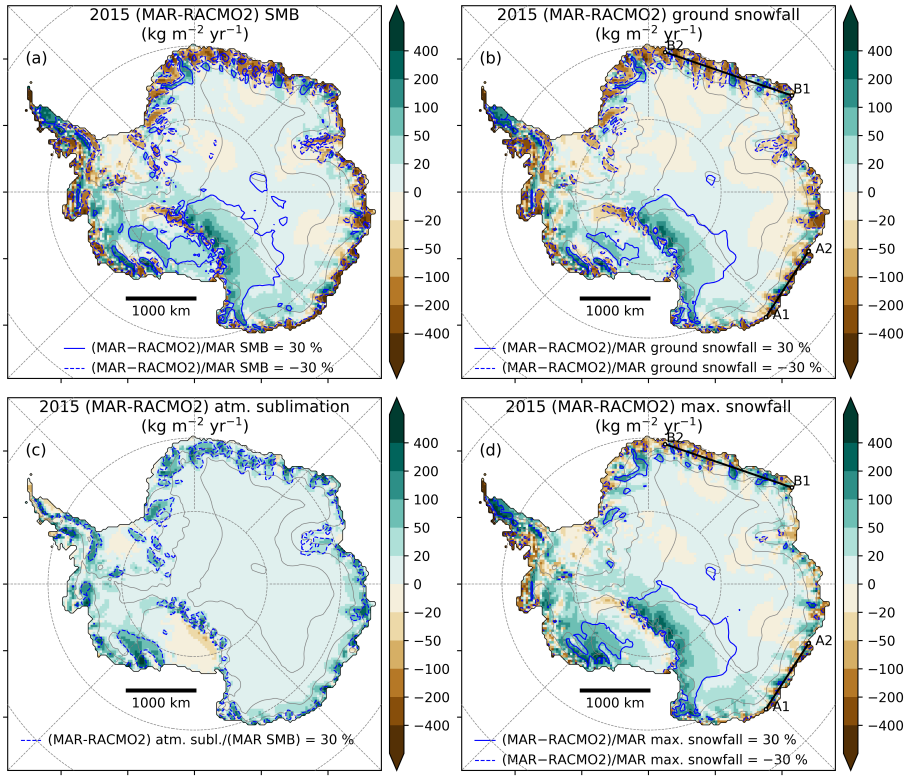

Figure 5. The four maps show mass fluxes in kg m^{-2} yr^{-1} for the year 2015. (a) Difference in SMB between MAR and RACMO2. Blue lines delimitate areas where the SMB difference is 30 % greater than MAR SMB, with solid lines when MAR is greater than RACMO2 and dashed lines when MAR is lower than RACMO2. (b) Same as a) but for the snowfall amounts at the ground. (c) Same as a) but for the sublimation of precipitation in the atmospheric layers. ~~Brown colours and dashed line are for MAR atmospheric sublimation greater than RACMO2 atmospheric sublimation.~~ (d) Same as a) but for the maximum snowfall amount (equal to ground snowfall plus atmospheric sublimation). Locations of transects A1-A2 and B1-B2 extracted in Fig. 6 are shown in panels b) and d).

To deepen this analysis, we re-ran MAR for the year 2015 in order to save the full atmosphere snowfall fields. From the daily 3D snowfall amounts, we derived the atmospheric sublimation amount from the difference between the maximum snowfall and the ground snowfall in each atmospheric column, as in Grazioli et al. (2017). The same was done for RACMO2. We find that the atmospheric sublimation simulated by MAR (363 Gt for the year 2015 over the grounded ice sheet) is higher than estimated in Grazioli et al. (2017) (299 Gt after interpolation on the same mask), and much higher than simulated by RACMO2 (128 Gt, Fig. 5c). A major difference between MAR and RACMO2 is the advection of precipitation in the atmosphere: in MAR, precipitating particles are explicitly advected through the atmospheric layers until they reach the surface, while in RACMO2, precipitation is added to the surface without horizontal advection, and is able to interact with the atmosphere only in a single time step ~~only~~ (6 min in this simulation). Consequently, atmospheric sublimation is likely to be underestimated in RACMO2.

We conclude, in agreement with Grazioli et al. (2017), that atmospheric sublimation is a major mass sink at the ice sheet margins in MAR, as for the year 2015 it represents 16 % of the snowfall loaded on the grounded ice sheet (12 % in Grazioli et al., 2017), and 26 % for areas bellow 1000 m ~~asl~~ a.s.l. (17 % in Grazioli et al., 2017).

It is noticeable that very few SMB observations are available in areas where Grazioli et al. (2017) identify low-level sublimation, marked by magenta bands in Fig. 2. Except for Ross–Marie Byrd Land, the only other areas where low-level sublimation is greater than 15 % of the total precipitation as defined by Grazioli et al. (2017) are close to Dumont d'Urville (coastal Adelie Land) and to Syowa (coastal Dronning Maud Land). In those areas the SMB amount is indeed larger in RACMO2 than in MAR and in observations. Both RCMs overestimate SMB around 2000 m a.s.l. in Dronning Maud Land and in Ross–Marie Byrd Land (Fig. 2), which could indicate katabatic channels not enough resolved by the topography of the models.

3.4 Precipitation formation and advection

Differences between MAR and RACMO2 snowfall fields are strongly reduced when considering the maximum snowfall amounts (before sublimation in the low-level atmosphere) rather than the ground snowfall amounts (Fig ~~5b–d~~. 5b and Fig. 5d). However, MAR snowfall rates generally exceed those simulated by RACMO2, by more than 30 % on the lee side of the West AIS (Marie Byrd Land toward Ross ice shelf), on the lee side of the Transantarctic Mountains (Victoria Land) and close to crests at the ice sheet margins. MAR maximum snowfall rates are lower than simulated by RACMO2 windward of topographic barriers and in valleys at the ice sheet margins. This spatial pattern looks similar to the one obtained in RACMO2 when delaying the conversion of cloud ice/water into snow/rain (Fig. 3a of van Wessem et al., 2018). This change led to both ice and water clouds lasting longer in the atmosphere before precipitating and therefore being advected further towards the ice sheet interior (van Wessem et al., 2018).

For a more in-depth analysis, we extract MAR and RACMO2 snowfall rates on two transects at the ice sheet margins (Fig. 6), following the main wind direction during cyclonic activities (locations shown in Fig. 5~~b–d~~b and Fig. 5d). On these transects the observed difference in maximum snowfall between MAR and RACMO2 is largely explained by a phase difference in the snowfall peaks windward of the topographic barriers, with MAR peaking closer to the crests than RACMO2 (Fig. 6b). This induces a wave-like pattern of precipitation difference strongly related to the shape of the topography, with larger snowfall amounts in MAR than in RACMO2 just windward of crests, and lower snowfall amounts in MAR than in RACMO2 around windward valleys. At the ground, lower snowfall in MAR than in RACMO2 in valleys is amplified by low-level atmospheric sublimation which peaks in katabatic channels (Fig. 6c).

Observations do not enable to definitively discriminate one model against the other, but we observe a general tendency for MAR to overestimate accumulation on Ross–Marie Byrd Land and close to ice sheet summits (Dome C, Dome A, Dome F, see Fig. 1d and Fig. 2). Close to summits the wind is low, so missing drifting snow transport process is unlikely explanation for a positive bias in SMB modelled by MAR (Fig. 4b). Over the Greenland ice sheet, MAR tends to overestimate ice cores based accumulation inland (Fettweis et al., 2017) while RACMO2 underestimates it (Noël et al., 2018).

We conclude that the differences in MAR and RACMO2 snowfall patterns are very likely related to differences in the advection of precipitation inland, which may arise from (i) the different advection of precipitating particles to the ground

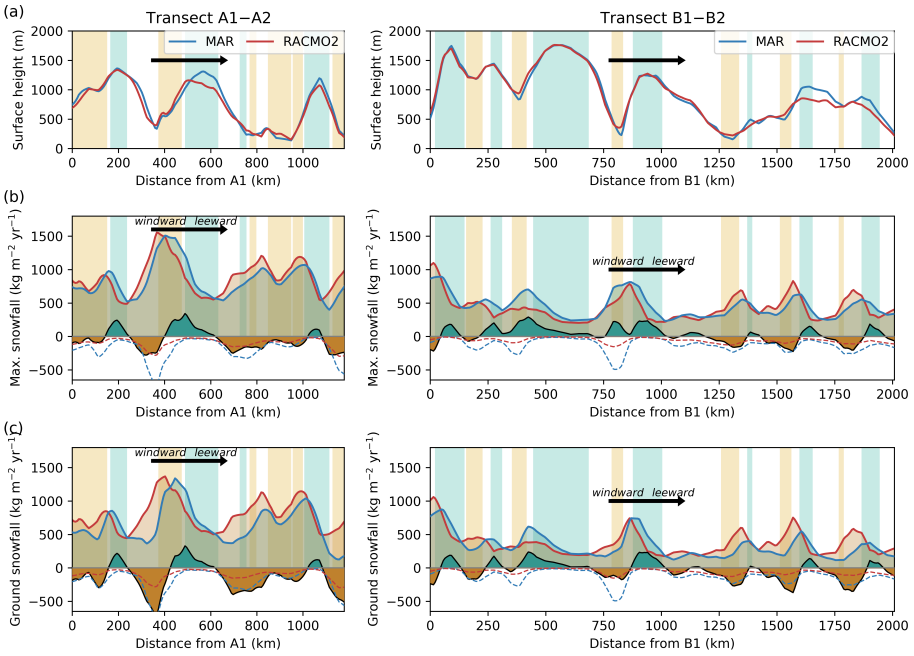

Figure 6. MAR and RACMO2 simulated fields for the year 2015, extracted with a bi-linear interpolation for (left) transect A1-A1 and (right) transect B1-B2 (locations shown in Fig. 5~~b-d~~b and Fig. 5d). Each panel shows MAR fields (blue lines) and RACMO2 fields (red lines) for (a) surface height, in m ~~asl~~a.s.l.; (b) maximum snowfall amounts, equal to ground snowfall plus atmospheric sublimation, in kg m^{-2} yr^{-1}; and (c) snowfall amounts at the ground, in kg m^{-2} yr^{-1}. In (b) and (c), the thick black line is for the difference in snowfall between MAR and RACMO2 (MAR-RACMO2), with green-filled areas when MAR snowfall is larger than RACMO2 snowfall, and brown-filled areas when MAR snowfall is lower than RACMO2 snowfall (same convention as in Fig. 5); the dotted lines are for the atmospheric sublimation modelled by MAR (blue) and by RACMO2 (red), negative when it induces a decrease in precipitation; light coloured bands show crests (light blue, curvature of MAR topography greater than 0.005 10^{-6} m^{-1}) and valleys (light yellow, curvature of MAR topography lower than -0.005 10^{-6} m^{-1}). The thick black arrows show the main 800 hPa wind direction during cyclonic activity.

described in Section 3.3, (ii) different timing of precipitation formation (cloud/precipitation conversion thresholds), and/or (iii) different dynamical response to the topographic forcing, caused either by different dynamical cores or by the different resolutions (the 27 km resolution in RACMO2 better resolves the ice sheet topography than the 35 km resolution in MAR).

4 Discussion and conclusion

In our study, we evaluate new estimates of the Antarctic SMB obtained with the polar ~~RCM MAR run~~ regional climate model MAR ran for the first time for decades-long simulations at the scale of the whole Antarctic ice sheet. We use model settings comparable to previous MAR simulations over Greenland (Fettweis et al., 2017) but with a specific upper atmosphere relaxation and new surface snow density and roughness length parameterisations. We present ~~the dynamical downscaling of~~ simulations

of MAR forced by ERA-Interim, JRA-55 and MERRA2 ~~with MAR~~ for the satellite era (1979-2015) where we can rely on reanalyses products. Remarkably, MAR forced by those three reanalyses give similar spatial and temporal SMB patterns. We also compare MAR with the latest simulations of the RCM RACMO2 forced by ERA-Interim (van Wessem et al., 2018). We find no significant differences between MAR and RACMO2 SMB when integrated on the AIS and its major basins (Table 2).

As the dominant feature of the Antarctic SMB is its strong ~~coast to plateau~~ coast-to-plateau gradient, we extract stake transects and sectors with large elevation ranges from the GLACIOCLIM-SAMBA SMB observational dataset. We show that both RCMs show similar performances when compared to observations, with a good representation of the SMB gradient (Fig. 2). But more importantly, we outline and quantify missing or underestimated processes in both RCMs.

Along stake transects, we relate 100 km-scale fluctuations of observations around the smooth modelled SMB pattern to the shape of the ice sheet captured on the 35×35 km MAR grid. Both RCMs accumulate too much snow on crests, and not enough snow in valleys, as a result of drifting snow transport fluxes not included in MAR and probably underestimated in RACMO2 by a factor of three (Fig. 4). In the RACMO2.3p2 version used here, the modified drifting snow routine induced almost halved drifting snow transport and sublimation fluxes compared to the previous RACMO2.3p1 version (Lenaerts and van den Broeke, 2012). In a recent study combining satellite observation of drifting snow events and reanalysis products, Palm et al. (2017) estimate the drifting snow sublimation to be about $\sim$393 $\mathrm{Gt\ yr^{-1}}$ over the Antarctic ice sheet, vs. 181 $\mathrm{Gt\ yr^{-1}}$ in RACMO2.3p1 and 102 $\mathrm{Gt\ yr^{-1}}$ in RACMO2.3p2 (van Wessem et al., 2018). Consequently, observational constraints from our study and from Palm et al. (2017) both tend to confirm that drifting snow transport and sublimation fluxes are likely much larger than previous model-based estimates and need to be (better) resolved and constrained in climate models.

We also point out that MAR generally simulates larger SMB and snowfall amounts than RACMO2 inland, particularly on the lee side of ~~topographic barriers~~ the Transantarctic Mountains and on crests at the ice sheet margins, whereas MAR simulates lower snowfall than RACMO2 windward of ~~topographic barriers and in valleys at the ice sheet margins~~mountain ranges and promontories. Sublimation of precipitating particles in low-level atmospheric layers is largely responsible for the significantly lower snowfall rates in MAR than in RACMO2 in valleys at the ice sheet margins. As precipitating snow particles have larger time residence in the atmosphere in MAR than in RACMO2 (Section 3.3), amounts of precipitation lost by sublimation in katabatic channels are more than twice as much in MAR as in RACMO2. The remaining spatial differences in snowfall between MAR and RACMO2 are attributed to differences in advection of precipitation, snowfall particles being likely advected too far inland in MAR.

Atmospheric sublimation represents 429 $\mathrm{Gt\ yr^{-1}}$ in MAR over the whole AIS (Peninsula excluded) for the year 2015, 89 % of which is lost below 2000 m ~~asl~~a.s.l., and 61 % below 1000 m ~~asl.~~a.s.l.. This might be of importance for the mass balance of glacier drainage basins (SMB minus discharge, Rignot et al., 2008; Shepherd et al., 2018), as ice streams are typically channel-shaped areas affected by low-level sublimation of precipitation. Consequently, we note the importance of saving precipitation fluxes in models at least 1300 m above the ground for comparison with CloudSat products, but ideally at all model levels below 1500 m above the ground to be able to compute sublimation of precipitation in the low-level atmospheric layers. This will become a standard output in forthcoming MAR simulations.

We expect that accounting for drifting snow in MAR will lead to significant improvements in describing the Antarctic SMB and surface climate, as it will enable (1) a quantification of the drifting snow sublimation mass sink, (2) a more realistic representation of relative humidity and temperature in the boundary layer, and (3) an explicit modelling of the drifting snow transport from crests to valleys. Exploring the impact of horizontal and vertical model resolution on drifting snow estimates and on sublimation of precipitation in katabatic channels will also be of importance as those processes are related to the shape of the ice sheet and to the advection of precipitation in the atmosphere. The accuracy of the topography has to be considered as well, as digital elevation models are in constant improvement over the Antarctic ice sheet (e.g. Slater et al., 2018) and should be regularly updated in climate models.

Code and data availability. Python scripts developed for this study as well as all required data are available at https://gitlab.com/cecileagosta/antarctica-smb-20c.git. The last version of MAR is freely distributed at http://mar.cnrs.fr/. Monthly MARv3.6.4 outputs from this study are freely available at ftp://ftp.climato.be/fettweis/MARv3.6/Antarctic/, together with the associated MAR source code. The ECMWF reanalyse ERA-Interim 6-hourly outputs were downloaded from http://apps.ecmwf.int/datasets/. The MERRA2 reanalyse 6-hourly outputs were downloaded from https://disc.sci.gsfc.nasa.gov/. The JRA-55 reanalyse 6-hourly outputs were downloaded from https://rda.ucar.edu/datasets/dS728.0/.

Author contributions. Cécile Agosta set-up the MAR model for Antarctica with several adaptations, performed model simulations and analysed model outputs and observations. Cécile Agosta, Anais Orsi, Xavier Fettweis and Vincent Favier designed the study. Cécile Agosta, Xavier Fettweis, Hubert Gallée, Charles Amory and Christoph Kittel developed the MAR model and contributed to the MAR set-up and output analyses. Xavier Fettweis and Hubert Gallée are the main developer of the MAR model. Michiel R. van den Broeke, J. Melchior van Wessem, Jan T.M. Lenaerts and Willem Jan van de Berg contributed to RACMO2 output analyses. All authors contributed to discussions in writing this manuscript.

Competing interests. The authors declare that they have no conflict of interests.

Acknowledgements. We thank Kenichi Matsuoka, Massimo Frezzotti and the second anonymous reviewer for their constructive and insightful comments, that led to a much improved paper. Cécile Agosta performed MAR simulations during her Belgian Fund for Scientific Research (F.R.S.-FNRS) research fellowship. Computational resources have been provided by the Consortium des Équipements de Calcul Intensif (CÉCI), funded by the F.R.S.-FNRS under Grant No. 2.5020.11. We acknowledge Jacopo Grazioli for sharing low-level sublimation product and his expertise of this dataset. We acknowledge Yetang Wang for sharing his updated version of the GLACIOCLIM-SAMBA dataset. We acknowledge Christophe Genthon for fruitful discussions and suggestions. The authors acknowledge the support from Agence Nationale de la Recherche scientific for the scientific traverses in Antarctica and the associated research on climate and surface mass balance modeling, projects ANR-14-CE01-0001 (ASUMA) and ANR-16-CE01-0011 (EAIIST).

Supplementary: Estimation of the Antarctic surface mass balance using the regional climate model MAR (1979-2015) and identification of dominant processes

Cécile Agosta[1,2,3], Charles Amory[1], Christoph Kittel[1], Anais Orsi[2], Vincent Favier[3], Hubert Gallée[3], Michiel R. van den Broeke[4], Jan T.M. Lenaerts[4,5], J. Melchior van Wessem[4], Willem Jan van de Berg[4], and Xavier Fettweis[1]

[1]F.R.S.-FNRS, Laboratory of Climatology, Department of Geography, University of Liège, B-4000 Liège, Belgium
[2]Laboratoire des Sciences du Climat et de l'Environnement (IPSL/CEA-CNRS-UVSQ UMR 8216), CEA Saclay, F-91190 Gif-sur-Yvette, France
[3]Université Grenoble Alpes, CNRS, Institut des Géosciences de lEnvironnement, F-38000, Grenoble,France
[4]Institute for Marine and Atmospheric Research Utrecht, Utrecht University, Utrecht, the Netherlands
[5]Department of Atmospheric and Oceanic Sciences, University of Colorado Boulder, Boulder CO, United States of America

December 27, 2018

Table S1: References of snow density datasets~~and~~. For each depth range, we give the total number of observations ~~/~~(left) and the number of 35×35 km model grid cells ~~by depth range~~they cover (right).

Reference	Dataset	0–20 cm	0–50 cm	0–100 cm
Albert et al. (2007)	SUMup17 [1]	3/1	3/1	3/1
Brucker and Koenig (2011)	SUMup17 [1]	6/5	6/5	6/5
Cameron et al. (1968)	Kaspers04 [2]	0/0	0/0	22/22
Ding et al. (2011)	CHINARE	568/39	0/0	0/0
Fujiwara and Endo (1971)	JARE69	65/38	0/0	13/13
Gallet et al. (2011)	DC-DDU08	8/8	7/7	0/0
Herron and Langway (1980)	Kaspers04 [2]	0/0	1/1	1/1
Kaspers et al. (2004)	Kaspers04 [2]	0/0	2/2	2/2
Kreutz et al. (2011)	SUMup17 [1]	1/1	1/1	1/1
Medley et al. (2013)	SUMup17 [1]	1/1	3/3	2/2
Sugiyama et al. (2012)	JASE07	0/0	43/43	43/42
Watanabe (1975)	JARE70	6/1	6/5	8/5
van den Broeke et al. (1999)	Kaspers04 [2]	0/0	8/8	8/8

[1] Montgomery et al. (2018), [2] Kaspers et al. (2004)

Table S2: Estimates of drifting snow transport fluxes summed over the total (TIS, 13.4 10^6 km^2) and the grounded (GIS, 12.0 10^6 km^2) Antarctic ice sheet, excluding Peninsula. Parenthesis (α_{max},ws_{min},ws_{max}) are for estimates of drifting snow transport based on a scaling of the curvature: drifting snow transport (kg m^{-2} yr^{-1}) = α (10^6 kg m^{-1} yr^{-1}) × curvature (10^{-6} m^{-1}), with $\alpha = 0$ (10^6 kg m^{-1} yr^{-1}) for wind speed lower than ws_{min} (m s^{-1}), $\alpha = \alpha_{max}$ (10^6 kg m^{-1} yr^{-1}) for wind speed greater than ws_{max} (m s^{-1}), and α linearly increasing as a function of wind speed in between. Wind speed is the annual average of 10 m wind speed of MAR forced by ERA-Interim.

Component	(3700,5,9)	(3700,6,8)	(4700,5,9)	(2700,5,9)	RACMO2
TIS w/o Peninsula					
Mass loss (Gt yr^{-1})	82	81	95	66	21
Mass gain (Gt yr^{-1})	74	74	88	58	16
Net (Gt yr^{-1})	8	7	7	8	5
GIS w/o Peninsula					
Mass loss (Gt yr^{-1})	81	80	94	65	19
Mass gain (Gt yr^{-1})	68	69	81	53	14
Net (Gt yr^{-1})	13	11	13	12	5

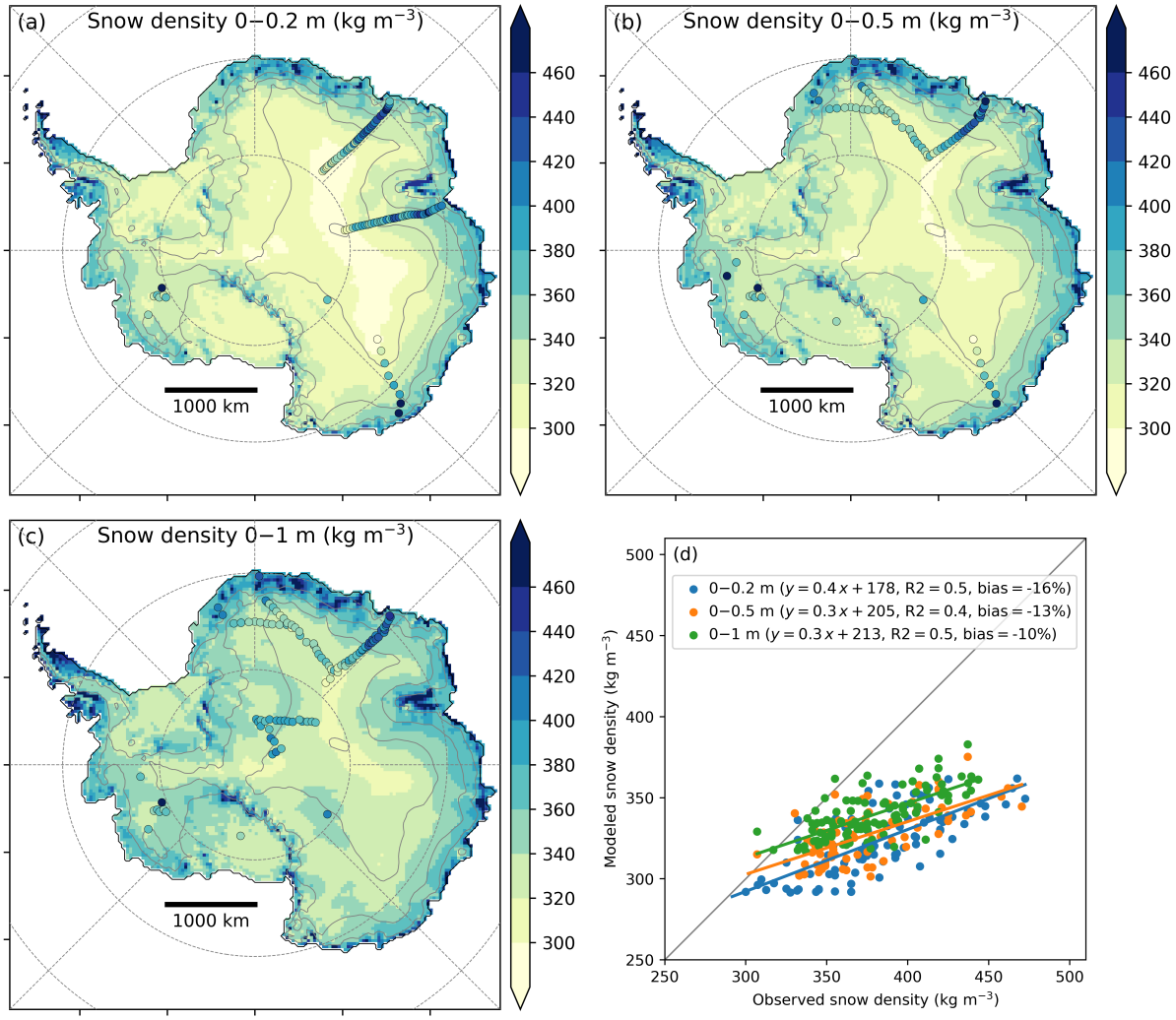

Figure S1: Snow density modelled by MAR (maps) and observations (dots) for (a) the first 20 cm of snow, (b) the first 50 cm of snow and (c) the first meter of snow, and (d) shows scatterplot of modelled versus observed snow density. The snow density database is detailed in Table ~~S2~~S1. Modelled snow density is taken in average for the period 1979-2015. Observed snow density is averaged on MAR grid cells.

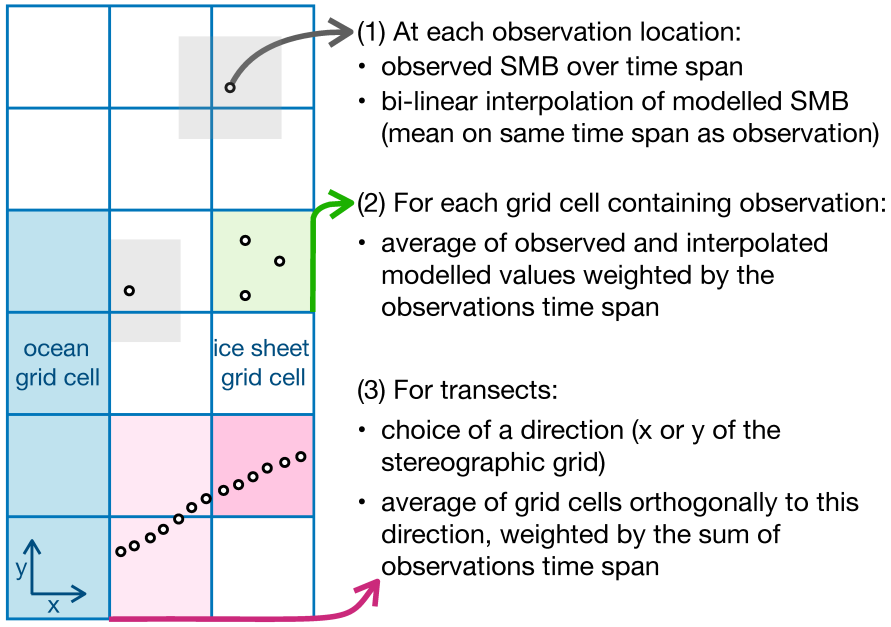

Figure S2: Sketch explaining the comparison method between observed (points) and modelled (gridded) SMB.

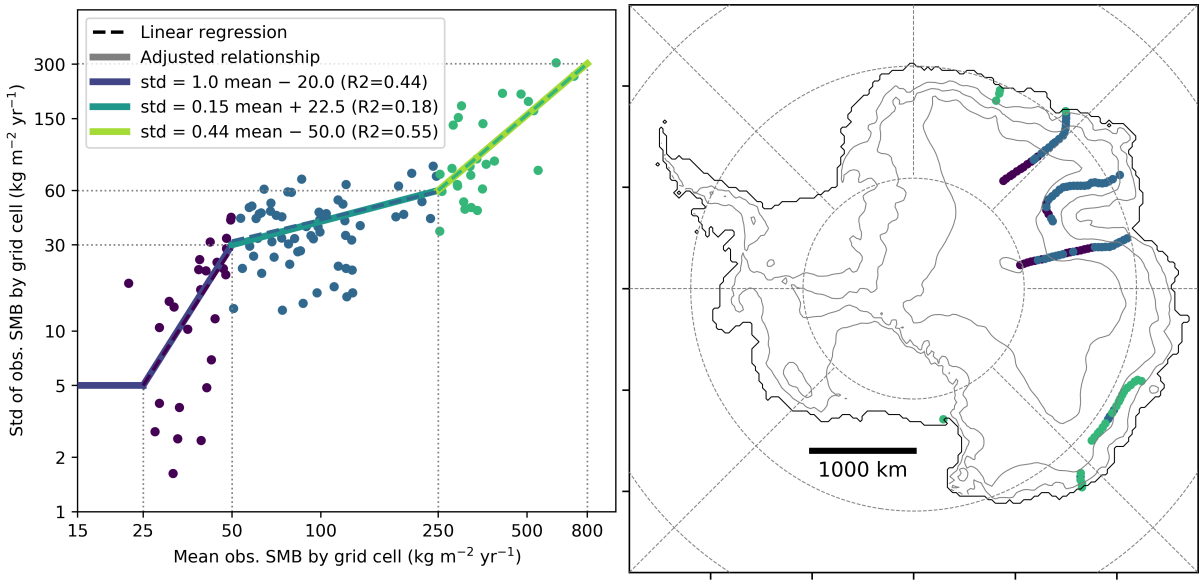

Figure S3: Estimate of the SMB spatial variability into 35 km×35 km grid cells as a function of mean observed SMB in the grid cell. (a) Standard deviation versus mean value of observed SMB for each MAR grid cell containing more than 10 observations. We delimitate three variability regimes depending on mean SMB values : <=50 kg m^{-2} yr^{-1}, [50-250] kg m^{-2} yr^{-1} and >=250 kg m^{-2} yr^{-1}. (b) Location of the SMB regimes, with same colour code as in panel (a).

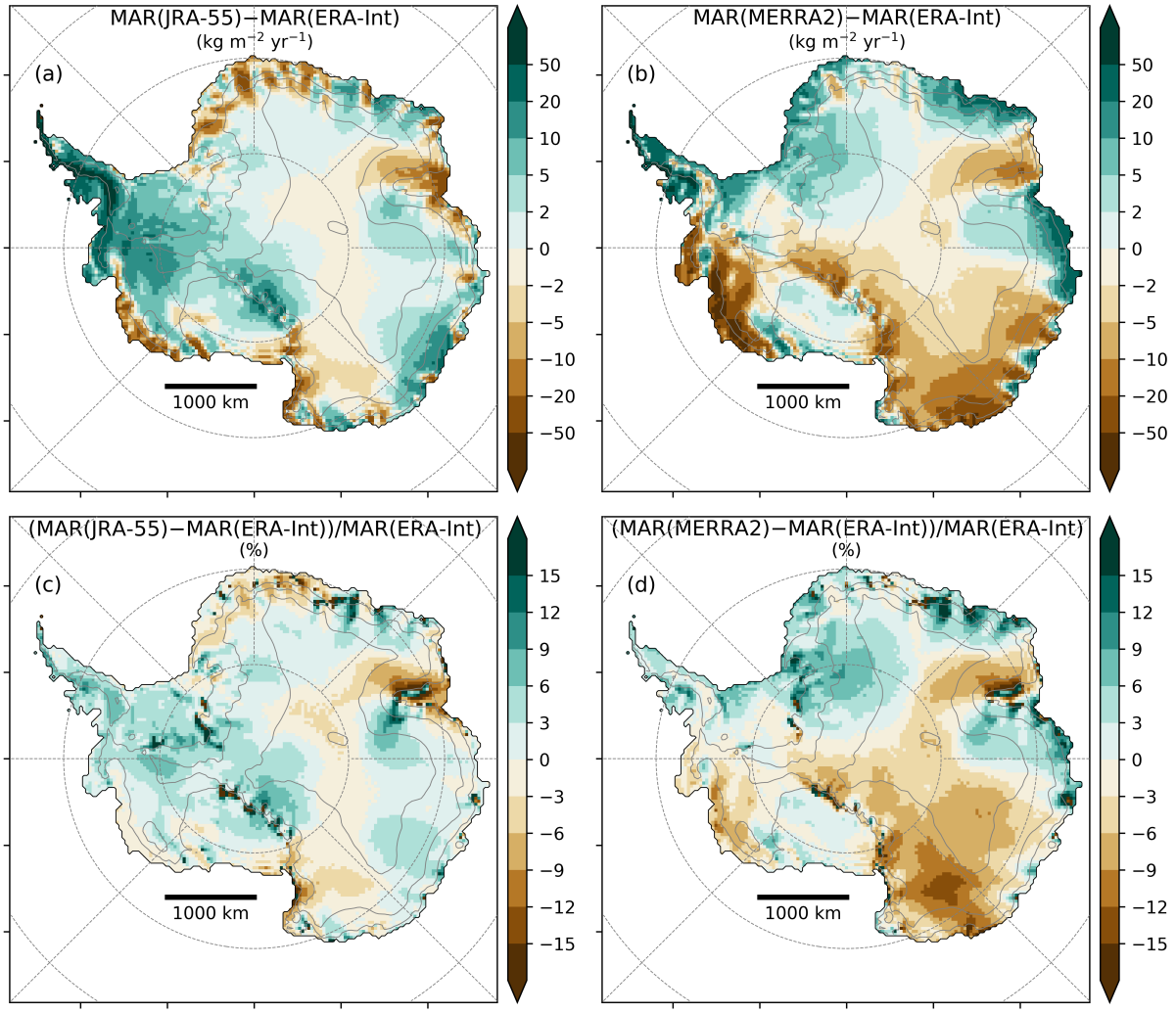

Figure S4: Difference between mean annual SMB modelled by MAR forced by (a) JRA-55 and (b) MERRA2 and MAR forced by ERA-Interim, for the period 1979-2015, in kg m^{-2} yr^{-1}. (c) and (d) are the same than (a) and (b) but divided by MAR(ERA-Interim) mean SMB (in %).

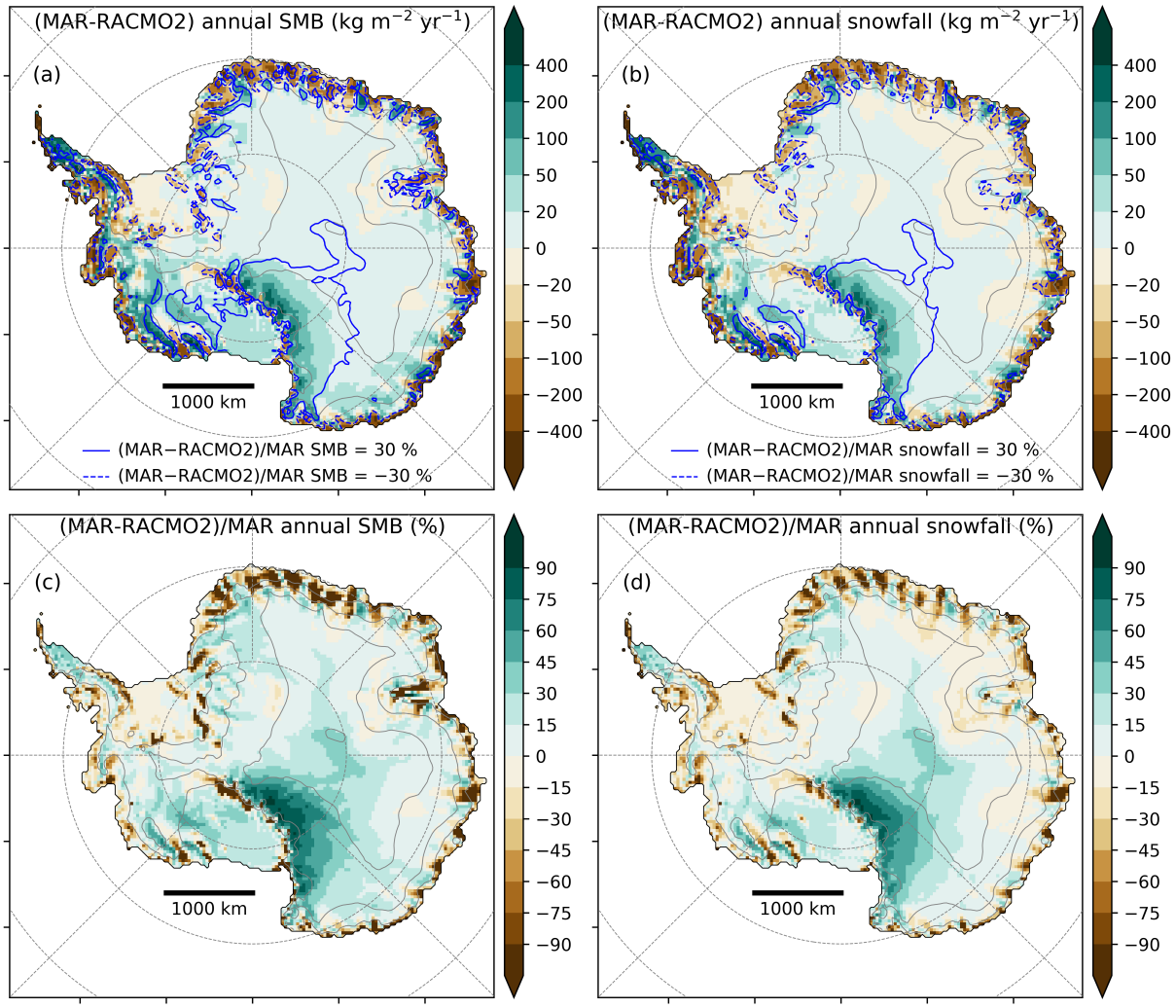

Figure S5: Difference between MAR and RACMO2 forced by ERA-Interim for the period 1979-2015 for (a-c) SMB and (b-d) snowfall. (a-b) Absolute differences, in kg m^{-2} yr^{-1}, and (c-d) relative differences, in %. In (a-b), blue lines delimitate areas where the SMB/snowfall difference is 30 % greater than MAR SMB/snowfall, with solid lines when MAR is greater than RACMO2 and dashed lines when MAR is lower than RACMO2.

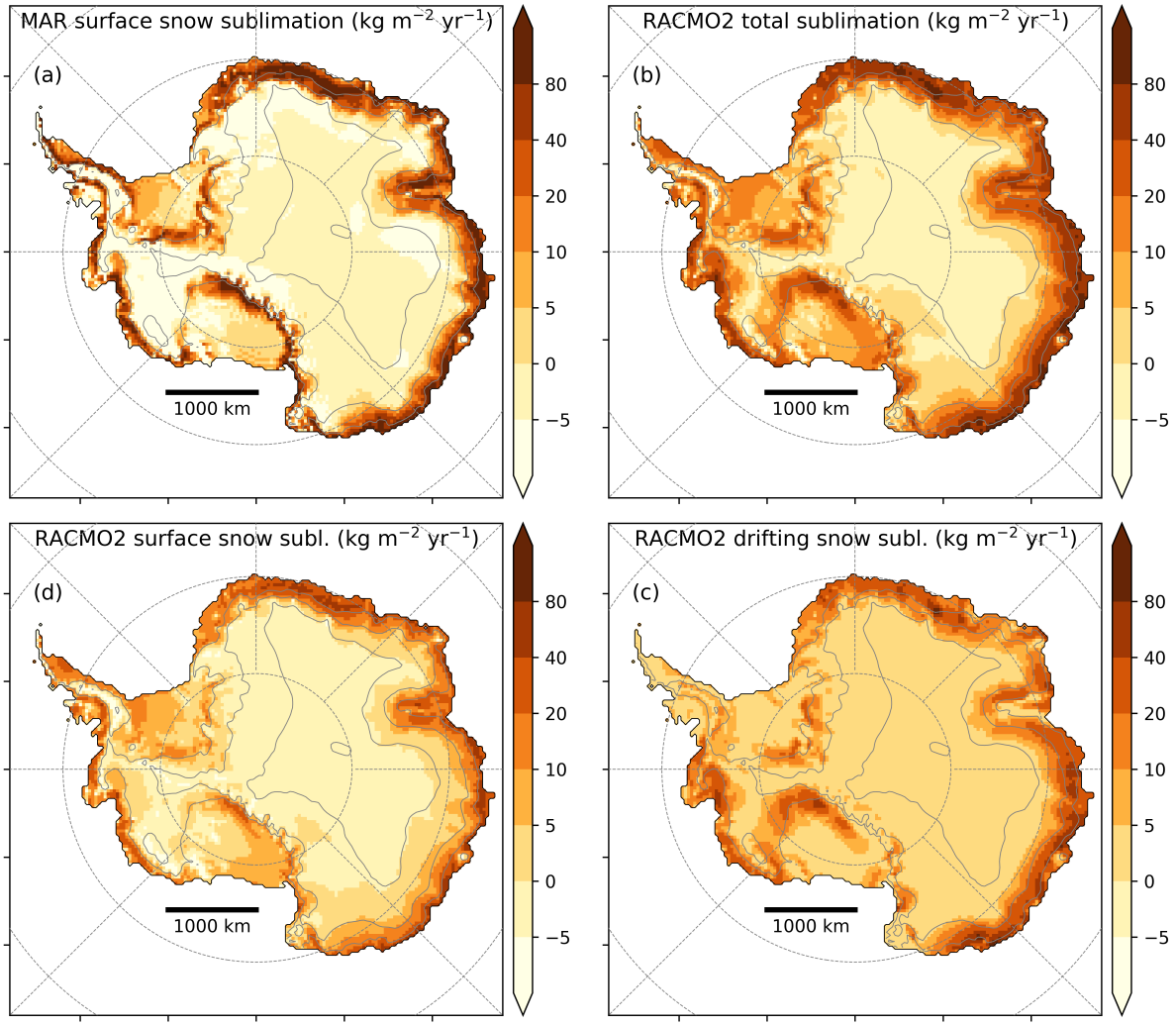

Figure S6: Annual mean modelled sublimation fluxes for the period 1979-2015, in kg m^{-2} yr^{-1}. (a) Sublimation at the surface of the snowpack modelled by MAR(ERA-Interim). (b) Total sublimation (surface snow sublimation plus drifting snow sublimation) modelled by RACMO2(ERA-Interim). (c) Same as (a) but for RACMO2(ERA-Interim). (d) Drifting snow sublimation modelled by RACMO2(ERA-Interim). MAR does not include drifting snow in these simulations.

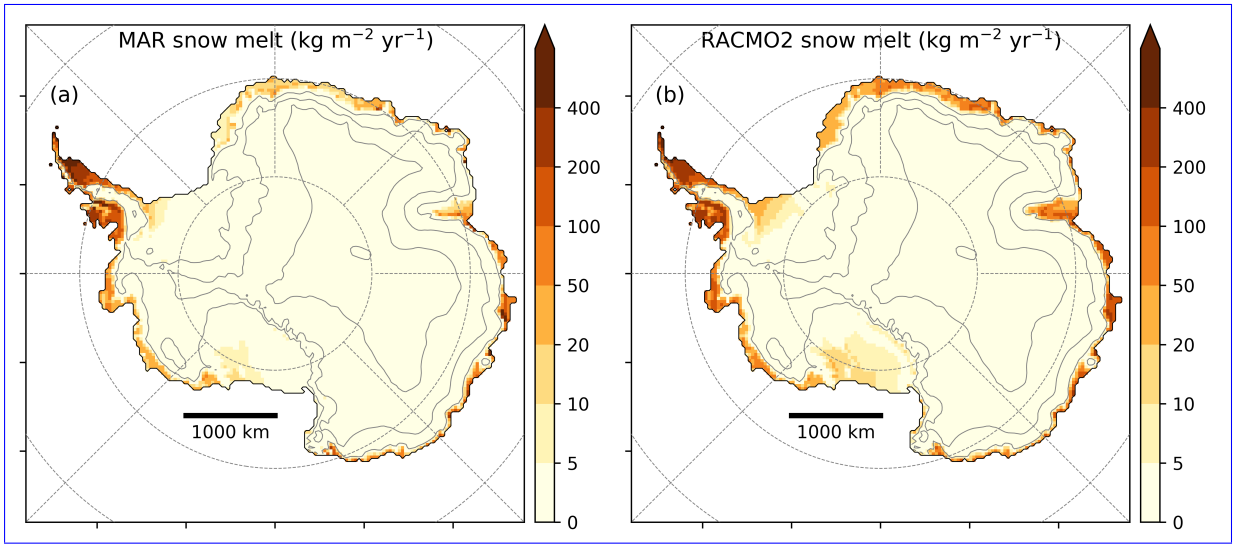

Figure S7: Snowmelt amounts modelled by MAR and RACMO2 forced by ERA-Interim for the period 1979-2015, in kg m^{-2} yr^{-1}. Note that snowmelt is almost totally refrozen in the snowpack in both models (Table ~~1~~2).

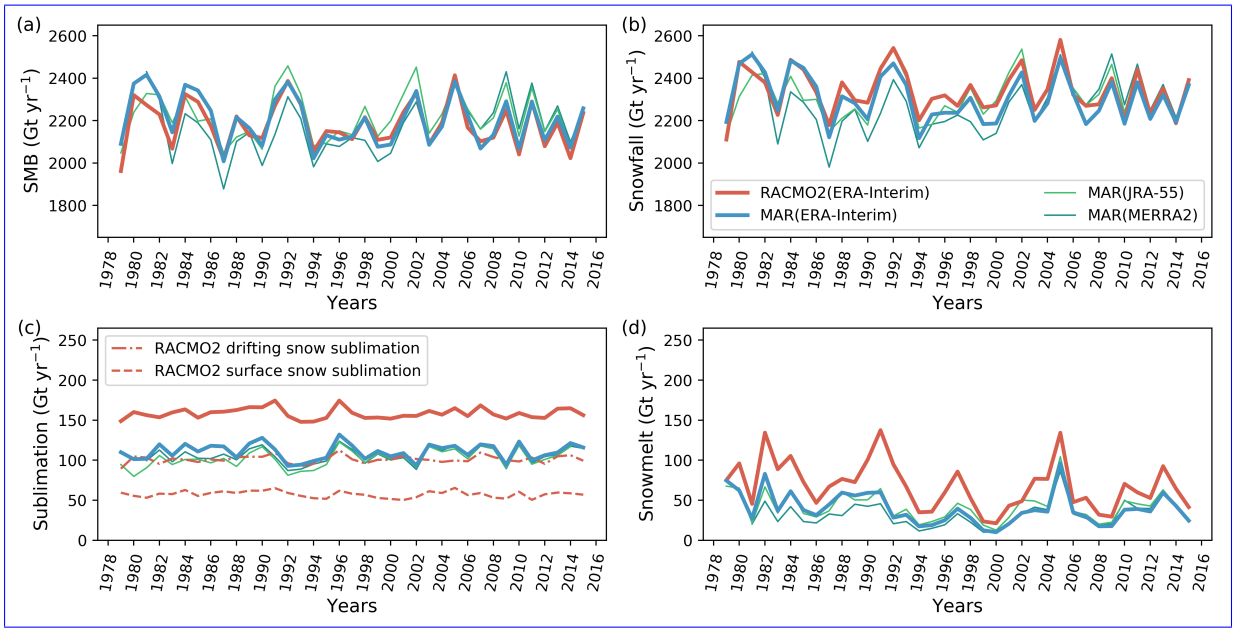

Figure S8: Annual SMB components summed over the Antarctic ice-sheet excluding peninsula (13.4 10^6 km^2), for (a) SMB, (b) snowfall, (c) sublimation and (d) snowmelt. Red solid thick line is for RACMO2(ERA-Interim), light green solid thin line is for MAR(ERA-Interim), blue solid thick line is for MAR(JRA-55) and dark green solid thin line is for MAR(MERRA2). Note that snowmelt is almost totally refrozen in the snowpack in both models (Table~~1~~ 2).

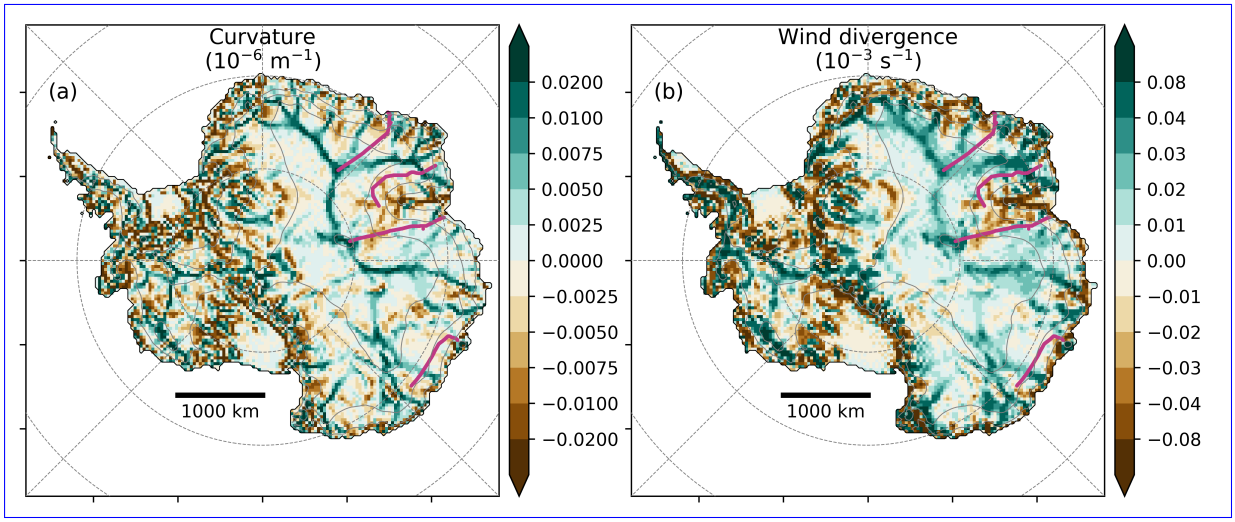

Figure S9: (a) Curvature of topography computed on the MAR grid (10^{-6} m^{-1}) (b) Divergence of the mean annual 10 m wind in MAR (m s^{-1} km^{-1})

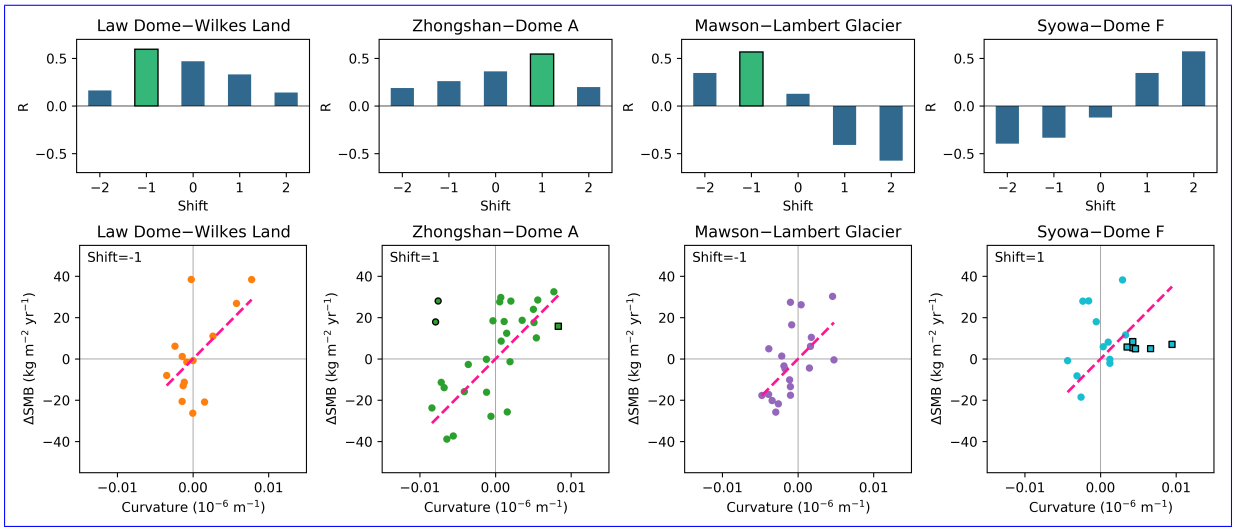

Figure S10: (top) Correlation coefficient R between MAR(ERA-Interim) SMB bias and curvature spatially shifted of -2, -1, 0, 1 and 2 grid cells. Green bars are for p-value lower than 0.05 and R greater than 0. (bottom) Scatterplots of MAR(ERA-Interim) SMB bias versus shifted curvature, with shift given at top left of each sub-figure. Pink dashed line is the regression line through origin computed for the four transects all-together (Fig. 4a). ~~Dots and squares with black contour lines are excluded from regression.~~ Squares are for locations where MAR annual 10 m wind speed in lower than ~~seven~~ 7 m s^{-1}. For the transect Zhongshan–Dome A, we excluded one data point with low wind speed (square with black outline) and two data points which were clear outliers (dots with black outlines). For the transect Syowa–Dome F, we excluded 5 data points with low wind speed (squares with black outlines).

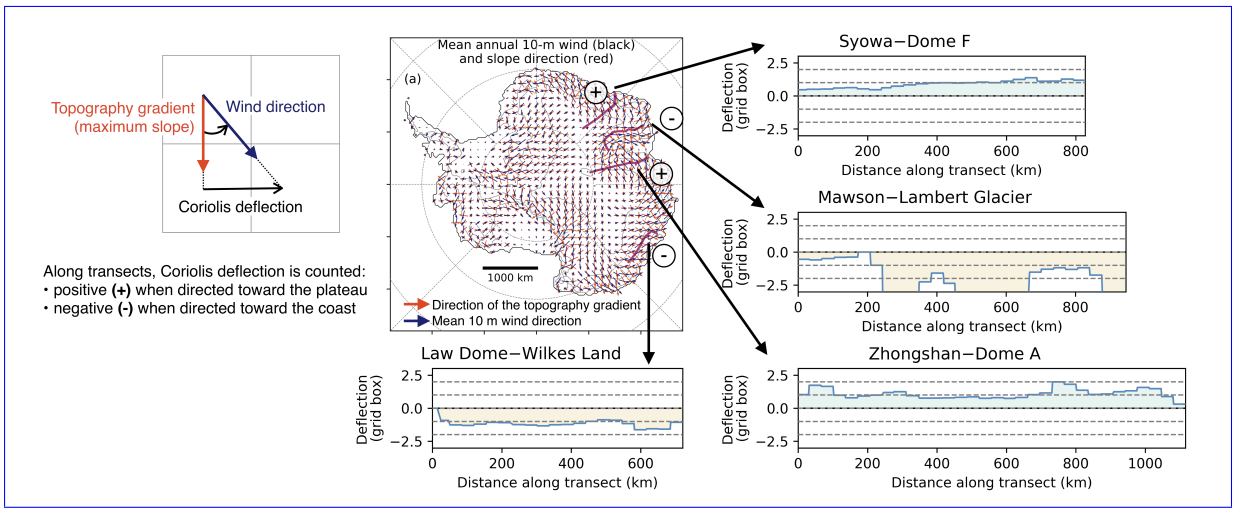

Figure S11: Estimate of the Coriolis deflection of the katabatic wind flow at the ice sheet surface. We compute the angle between the gradient of the topography (direction of the maximum slope) and the wind direction, and convert it in a deflection value, in percentage of the grid box size (deflection = tan(angle)). As transects are shown from the coast to the plateau, the Coriolis deflection sign is ~~given~~ counted along this same axis: a ~~positive sign when~~ deflection toward the coast shifts the wind ~~is deflected toward~~ backward in the ~~plateau~~axis (negative deflection), and a ~~negative sign when~~ deflection toward the plateau shifts the wind ~~is deflected toward~~ upward in the ~~coast along each transect~~axis (positive deflection). ~~Consequently~~Finally, as curvature of the topography is used as a proxy of wind divergence ~~,~~which drives the drifting snow transport, the shift of ~~the~~ curvature of +/- one grid cell according to the maximum of correlation with SMB bias (Fig. S10) is in agreement with the Coriolis wind deflection.

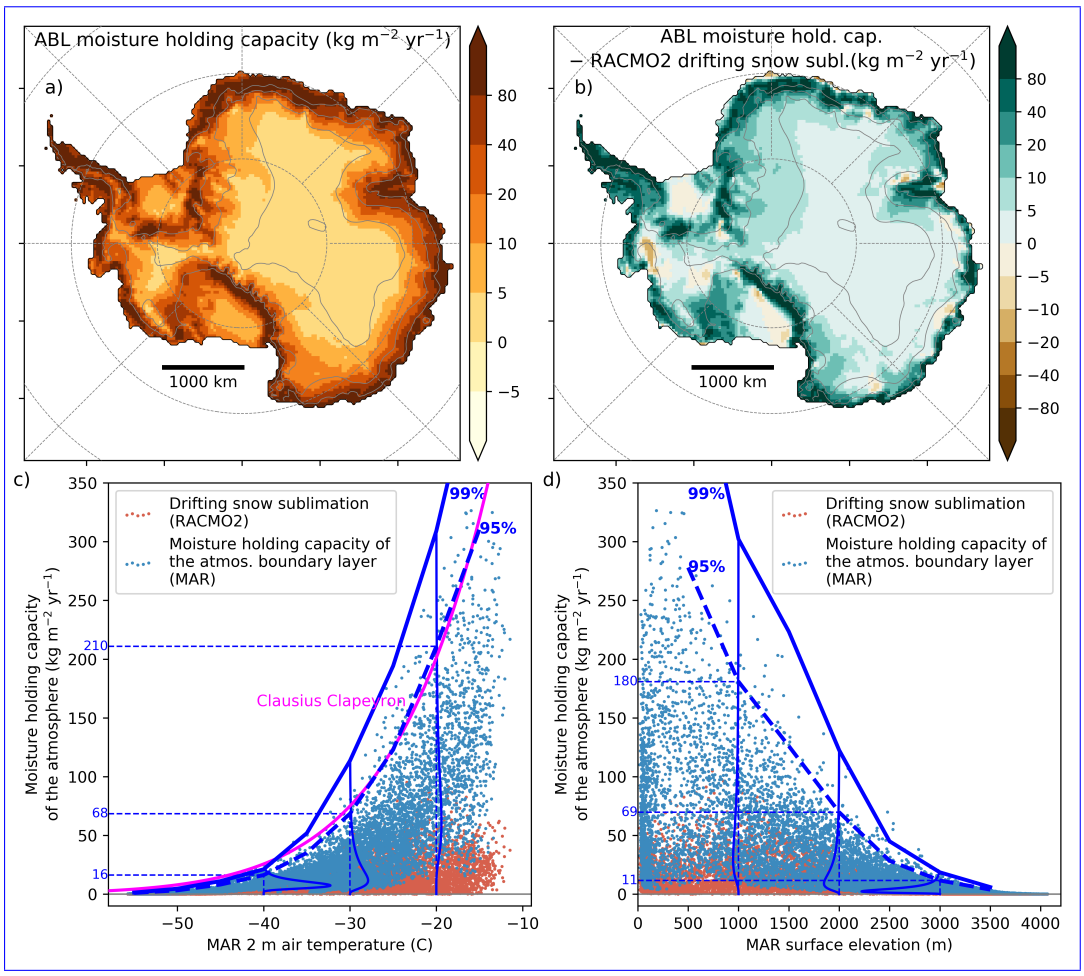

Figure S12: (a) Atmospheric boundary layer (ABL) moisture holding capacity in MAR for the year 2015, in kg m^{-2} yr^{-1}. The ABL moisture holding capacity is computed with daily variables: ABL moisture holding capacity $= \sum_{k=surface}^{k=ABLsummit}(Qsat-Q)\Delta P/g$, with Q the specific humidity, $Qsat$ the specific humidity at saturation, ΔP the pressure width of the atmospheric layer k and g the gravitational acceleration. We compute the top of the ABL as the level where the turbulent kinetic energy amounts to 1% of the turbulent kinetic energy maximum in the lowest layers of the model ~~(5% is used in Gallée et al. (2015))~~(5% is used in Gallée et al., 2015). We compute $Qsat$ using the relative humidity rh: $Qsat = Q/rh$. (b) Difference between the ABL moisture holding capacity in MAR and the drifting snow sublimation in RACMO2, for the year 2015, in kg m^{-2} yr^{-1} (c) ABL moisture holding capacity in MAR (blue dots) and drifting snow sublimation in RACMO2 (red dots), for the year 2015, in kg m^{-2} yr^{-1}, as a function of the mean 2 m air temperature in MAR, for the year 2015, in °C. The thin solid blue lines are normalised log-normal distribution of the ABL moisture holding capacity in MAR for 5°C temperature bins around -40°C, -30°C, and -20°C. The thick blue dashed line shows the 95% end of the distributions, and the thick blue solid line is the 99% end of the distributions. The pink line shows a Clausius-Clapeyron-like relationship with temperature: $y = exp(-L_s/R_v(1/ta - 1/ta_0) + log(subl_0))$, in kg m^{-2} yr^{-1}, with ta the air temperature in K, L_s the enthalpy of sublimation (2.8 10^6 J kg^{-1}), R_v the gas constant of water vapor (461.52 J kg^{-1} K^{-1}), ta_0 = 263.15 K and $subl_0$ = 500 kg m^{-2} yr^{-1}. (d) Same as (c) but for surface elevation instead of air temperature. Normalised distributions are computed for 500 m bins around 1000 m asl, 2000 m asl, and 3000 m asl. The ABL moisture holding capacity computed in the MAR model represents the maximum moisture amount that can be loaded in the atmospheric boundary layer according to the MAR simulations. We can confidently consider this ABL moisture holding capacity as an upper bound for drifting snow sublimation amounts (panels a and b), as MAR not including the drifting snow process implies that the ABL keeps its full potential to hold moisture. The ABL moisture holding capacity is exponentially dependent to the air temperature, following a Clausius-Clapeyron-like relationship (panel c).

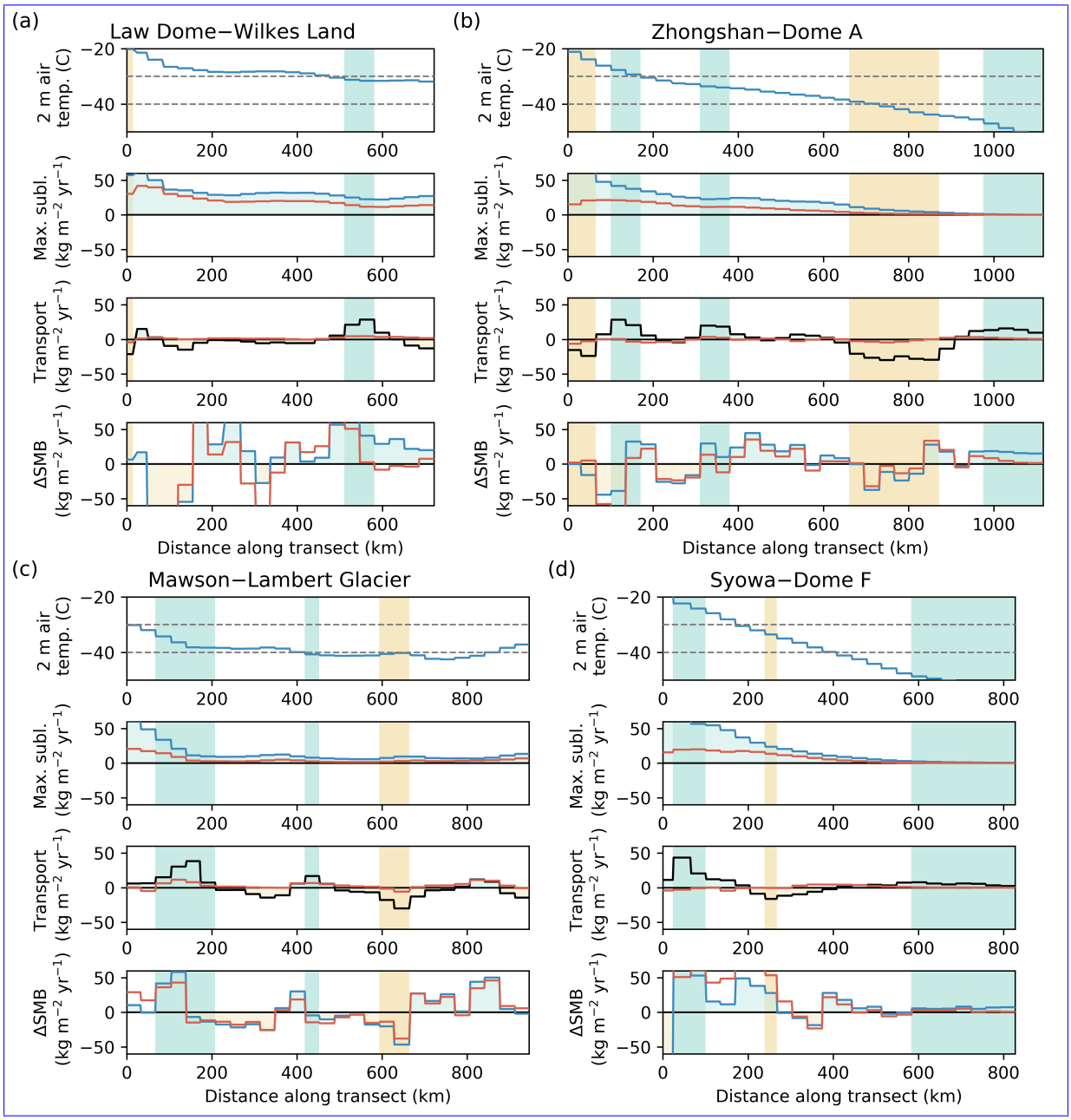

Figure S13: For each of the four long transects is shown, from top to bottom, for the year 2015: (top row) 2 m air temperature, in °C; (2nd row) atmospheric boundary layer moisture holding capacity in MAR (blue line), and drifting snow sublimation in RACMO2 (red line), in kg m^{-2} yr^{-1}; (3rd row) drifting snow transport estimate as a function of curvature (black line), and drifting snow transport simulated by RACMO2 (solid red line), in kg m^{-2} yr^{-1}; (bottom row) the difference between modelled and observed SMB for MAR (blue line) and RACMO2 (red line), in kg m^{-2} yr^{-1}. The blue bands are when the curvature of the topography is greater than 0.004 10^{-6} m^{-1} (crests) and yellow bands are when the curvature of the topography is lower than -0.004 10^{-6} m^{-1} (valleys).